Catalysis Today 286 (2017) 85–100

Contents lists available at ScienceDirect

Catalysis Today

journal homepage: www.elsevier.com/locate/cattod

The inhibitor role of NH_3 on its synthesis process at low temperature, over Ru catalytic nanoparticles

Charles Leterme, Camila Fernández, Pierre Eloy, Eric M. Gaigneaux*, Patricio Ruiz*

Institute of Condensed Matter and Nanosciences, Molecules, Solids and Reactivity (IMCN-MOST), Université catholique de Louvain, Place Louis Pasteur 1 bte L4.01.09, 1348 Louvain-la-Neuve, Belgium

ARTICLE INFO

Article history:
Received 30 April 2016
Received in revised form
21 December 2016
Accepted 3 January 2017
Available online 24 February 2017

Keywords:
Low-temperature processes
Ru particle size distribution
Ammonia decomposition
Ammonia synthesis
Catalytic cooperation

ABSTRACT

Single catalysts containing 3, 5 and 7 wt.% of Ru ($Ru3/Al_2O_3$, $Ru5/Al_2O_3$ and $Ru7/Al_2O_3$) were prepared via impregnation of alumina with RuO_2 colloidal suspensions. Two mechanical mixtures, containing $Ru3/Al_2O_3 + Ru5/Al_2O_3$ and $Ru3/Al_2O_3 + Ru7/Al_2O_3$, were also prepared. Catalytic activity was measured during low-temperature ammonia synthesis reaction. Three different tests were performed after reduction pretreatment of the catalysts: 1) Standard test, the catalytic activity of ammonia synthesis; 2) Test under $NH_3 + He$ treatment, following ammonia decomposition; 3) Test under $NH_3 + He + H_2$ treatment, following ammonia decomposition in presence of hydrogen. Standard tests were additionally used to study the effect of the different treatments ($NH_3 + He$ and $NH_3 + He + H_2$) on the catalytic activity of ammonia synthesis. Catalysts were characterized by N_2 physisorption, XRD and XPS spectroscopy. The size of Ru nanoparticles influences their performance during ammonia synthesis. The important role of the average size and size distribution of Ru nanoparticles in their activity for ammonia synthesis has been confirmed. Catalysts having a broad size distribution of Ru nanoparticles are more active than those having a narrow size distribution of Ru nanoparticles. Ammonia treatment has a negative effect in ammonia synthesis: results suggest that NH_x intermediates remaining strongly adsorbed on the surface inhibit the activity of catalysts during ammonia synthesis. The presence of hydrogen during NH_3 treatment inhibits ammonia decomposition and induces weaker adsorption of NH_x intermediates. The presence of large particles is necessary to reach and maintain a high catalytic activity during ammonia synthesis. Taking into account previous studies, it could be suggested that large Ru nanoparticles activates mobile hydrogen atoms that migrate towards small Ru nanoparticles, promoting NH_x hydrogenation. When mixing two catalysts having different mean Ru sizes, there is a significant synergistic effect in the catalytic activity, due to a more effective hydrogenation of NH_x intermediates.

1. Introduction

Ammonia synthesis is an industrial process that is well established in many countries since 1913. Ammonia synthesis has been a great input for the development of chemical industry. An enormous amount of research papers, reviews and monographs, ranging from theoretical studies to industrial applications, has been devoted to this process. Today, the development of advanced physicochemical characterization techniques (in-situ and 'operando' analysis, high resolution surface analysis, high resolution microscopy, etc.), DFT theoretical studies, more efficient tools for numerical analysis and more accurate tools for process simulation, allows a deeper understanding (at nanoscale level) of catalytic processes and mechanisms, which are the basis for the development of more active catalysts in order to carry out the reaction under more sustainable conditions.

Actually, the main challenge for ammonia synthesis is to perform the process at low 'near room' temperature and pressure. For this purpose, it is important to understand the reaction mechanisms and kinetics under these mild reaction conditions. Ru supported particles are the most studied catalytic system to perform the reaction under these conditions [1,2–3,4–5].

One aspect that has not been definitively resolved is the dependence of the catalytic activity on the Ru particle size. The catalytic performance has shown to be highly dependent on the size of Ru nanoparticles, although other factors can also have an important effect, such as the presence of promoters and the nature and electronic properties of supports. Most of the data reported in literature,

* Corresponding authors.
E-mail addresses: eric.gaigneaux@uclouvain.be (E.M. Gaigneaux), patricio.ruiz@uclouvain.be (P. Ruiz).

http://dx.doi.org/10.1016/j.cattod.2017.01.002
0920-5861/

however, correspond to studies performed at high temperature (>200 °C) and pressure (>30 bar) [6,7–8,9–10,11].

We have recently [12–14] demonstrated that the catalytic activity of Ru supported nanoparticles in low-temperature ammonia synthesis (<200 °C, 5 bar) increases with the mean size of Ru particles in the range 2–7 nm, confirming previous studies. Surprisingly, when studying catalysts prepared by different synthesis methods (impregnation, colloidal suspensions, microemulsion), quite different performances were observed for catalysts having the same mean size of Ru nanoparticles. More accurate and detailed nanoscopic characterization of the catalysts led to the conclusion that, contrary to what is commonly accepted, the size distribution of Ru nanoparticles is an important parameter to be considered when studying the effect of the metal particle size on the catalytic performance. Results demonstrated that ammonia synthesis is better conducted on alumina surfaces supporting Ru nanoparticles with a broad size distribution, ranging from very small (<2 nm) to large (about 10 nm) Ru nanoparticles. In fact, a catalytic cooperation exists between small and large Ru nanoparticles: small Ru nanoparticles expose the most active sites to (strongly) adsorb and dissociate N_2, but the rate of NH_x hydrogenation is low, which actually limits the reaction rate. Large Ru nanoparticles, meanwhile, activate hydrogen atoms that can more effectively hydrogenate NH_x species.

A mechanistic model of this cooperation has been experimentally confirmed and demonstrated by 'operando' DRIFTS analysis and H/D isotopic exchange. An activated dissociative adsorption of hydrogen on Ru/χ-Al2O3 can result from the interaction of OH groups with metal particles. Under low-temperature ammonia synthesis conditions, large Ru nanoparticles provide energetically favorable sites for the dissociative adsorption of hydrogen, activating H atoms with high diffusivity on alumina surface. On the contrary, hydrogen adsorption on small Ru particles leads to strongly attached H atoms presenting low diffusivity on alumina surface. H atoms can diffuse to the support and move along alumina surface via exchange with OH groups. A synergy in hydrogen mobility results between different-sized Ru particles in close proximity. A dynamic mechanism of catalytic cooperation is proposed to operate during low-temperature ammonia synthesis on polydispersed Ru nanoparticles supported on alumina. The mechanism involves transfer of H atoms from large Ru nanoparticles to nearby small particles. These H atoms can promote the catalytic activity in two different ways: (i) as reactants, directly hydrogenating reaction intermediates and releasing active sites, or (ii) as regulators of the local environment of active sites, keeping active sites (B_5-type sites) in optimal conditions for the dissociation of N_2 molecules with a low energy barrier. The identification of dynamic processes that may be involved in a catalytic reaction, under certain conditions, allows reformulating conventional kinetic models for a more accurate description of the process [15].

On the other hand, an Atomic Force Microscopy study demonstrated that the deposition of RuO_2 colloidal nanoparticles on a model support (freshly cleaved mica sheet) leads to supported Ru particles with different sizes: small RuO_2 clusters as well as larger nanorod-like structures exposing energetically favorable sites for hydrogen activation [16].

This puts into question the general, and very probably erroneous, approach to associate high catalytic activities with systems of monodisperse supported metallic particles, neglecting catalytic phenomena that might arise when particles of different sizes are simultaneously operating. The quantification of size distribution is essential for a correct interpretation of catalytic data. This oversimplification of the configuration and the size distribution of supported metallic nanoparticles is probably due to the difficulty (and probably the impossibility) to synthesize metallic nanoparticles homogeneously distributed on the surface of a support.

According to the thermodynamics, ammonia decomposition is reversible and endothermic and requires high temperature for complete conversion. Ammonia decomposes as follows:

$$2NH_3 \rightarrow N_2 + 3H_2 \qquad \Delta H = +46\,kJ\,mol^{-1}$$

Despite the reversibility of the reaction, new challenges arise in the decomposition path, especially at low reaction temperatures (<300 °C) due to the low thermodynamic equilibrium conversions. The equilibrium conversion close to 100% can be obtained at high temperature (in the range of 300–500 °C), At 300 °C equilibrium conversion is high (90%), but below 300 °C the equilibrium conversion drops significantly. At 100 °C the equilibrium conversion is about 28% and at 150 °C is 52%. Low temperature ammonia decomposition requires a catalyst that is active for the associative desorption of nitrogen adsorbed atoms.

However, to the best of our knowledge, there is no information in the literature concerning the effect of the ammonia produced on the catalytic performance during ammonia synthesis. Reported studies on ammonia decomposition mostly address the reaction mechanism, theoretical models and kinetics, the role of metal dopants, and the reactor performances.

Our previous studies showed that during ammonia synthesis, one of the steps in the reaction mechanism concerns the formation of some intermediate (NHx) adsorbed on the surface of the catalyst. As said above, the rapid hydrogenation of this intermediate is crucial to maintain high activity during ammonia synthesis. Large metallic supported nanoparticles promote hydrogenation of this intermediate. Our interest is to study the role of ammonia in catalytic activity. One of the steps of the mechanism of decomposition of ammonia is the formation of the adsorbed NHx intermediate. It thus seems logical to admit that the adsorption of ammonia could play a role in the rate of ammonia synthesis, precisely inhibiting the ammonia synthesis rate. In addition, as we have previously demonstrated that the size and size distribution of Ru nanoparticles play an important role in the synthesis of ammonia, it stands to reason to investigate if similar conclusion could be obtained in ammonia decomposition or more precisely in the NHx adsorption or catalyst deactivation. Then the first aim of this paper is to enlighten: i) the role of the ammonia formed during the ammonia synthesis process, ii) the role of the size of Ru nanoparticles in ammonia decomposition and adsorption and iii) to get some guidelines to control deactivation of catalyst by the presence of ammonia. To reach these objectives we have: i) first, to verify experimentally that in the catalytic system selected the cooperation between small and large particles operates during ammonia synthesis, ii) to use the same catalytic system to study the role of ammonia in the ammonia synthesis and iii) to measure the catalytic activity before and after particular treatment of the catalyst in presence of ammonia.

The study of NH_x reaction intermediates formed during ammonia synthesis could be the key to understanding the influence of the reverse reaction, since the same NH_x intermediates have been identified in the mechanism of ammonia decomposition. In addition, the size and size distribution of Ru nanoparticles might play an important role in ammonia decomposition, as it has been demonstrated for ammonia synthesis.

A particular experimental strategy has been selected. First, catalysts were prepared by deposition of a colloidal by suspension of RuO_2 nanoparticles of on alumina support. This method ensures a narrow size distribution of Ru supported nanoparticles. Catalysts with different loadings of Ru were selected in order to have catalysts with different mean sizes of Ru nanoparticles.

Nevertheless, the principal synthesis methods used to prepare metal supported catalysts leads to heterogeneity in the size of the metallic supported nanoparticles. Precipitation and impregnation do not allow efficiently controlling, at nanoscale, the surface con-

figuration and size distribution of catalytic supported crystallites. Sol-gel, citric and microemulsion methods allow a more accurate control of the particle size, but not the distribution of sizes. In fact it seems impossible to synthesize metal supported nanoparticles with a strict homogeneous size distribution. This is explained by the mechanism of nucleation and growing of the nanoparticles on the surface of a support [13,14]. This is a serious drawback to study the role of size and size distribution of particles. The colloidal method allows synthesizing RuO_2 nanoparticles with a controlled size and a very narrow size by distribution [17]. But, even using this method, the distribution is not homogeneous. In this work, the colloidal method was used expecting to obtain catalysts with different mean size of Ru particles and a narrow size distribution.

A standard catalytic test was selected to evaluate the activity of catalysts pretreated under different conditions, during ammonia synthesis. In order to get reproducible catalytic measurements, the synthesis and the standard test was performed 3 times for each catalyst. Two types of treatment were performed to the reduced catalysts, before the catalytic test: 1) treatment under ammonia + helium gas flow, in order to facilitate the adsorption of ammonia on the catalytic surface, and to study ammonia decomposition; 2) treatment under ammonia + hydrogen flow, in order to study the effect of H_2 on ammonia decomposition. The standard test was subsequently performed (after treatment 1 or 2) in order to study the effect of the corresponding treatments on the catalytic activity of ammonia synthesis. In addition, two catalysts were prepared by mechanically mixing two single catalysts, separately prepared. These mixtures were used to study how ammonia decomposition and its effect on the catalytic activity of ammonia synthesis changes with a broader size distribution of Ru particles.

The metal nanoparticles dispersed on an inert support play a crucial role in catalytic processes. It is well-recognized that the size of metal nanoparticles determines the activity and selectivity of the catalyst. It is also considered that in some cases the drastic change of catalytic properties of nanoparticles is due to their new properties (physical and chemical) that are created when their size decreases. One of the main difficulties to study the small metallic nanoparticles (below 3 nm) is to determine the exact size of these nanoparticles. The complications arise because particles are usually not spherical and their distribution on the support is not homogeneous. Moreover, some techniques are not useful because of the size limitation. In the case of an X-ray diffraction (XRD) study, the applicability is restricted by several factors such as the weight fraction or the size of crystallites. Indeed, it is established that the XRD technique is limited by the size of particles. In the case that the size of the particle is lower than 5 nm, no measurable signal is obtained by XRD. Mostly large crystallites are detected by XRD, which leads to an overestimation of the mean particle size. Size limitation is also the problem with Transmission electronic microscopy (TEM) measurements; in fact the detection is limited by contrast effects which may result in the difficulty to detect the small clusters containing a few atoms. Moreover, several images of the same sample on different zones have to be analyzed and distribution can be only statistically established by measuring a great number (about 1000) of particles. X-ray photoelectron spectroscopy (XPS) is a powerful tool to study the external surface of catalysts. XPS allows determining the chemical composition and the oxidation state of components present on the catalyst surface. In addition the sizes of the nanoparticles can be estimated from XPS data using an adequate modeling of the signal. Chemisorption measures the accessible surface sites while all of the other techniques measure the sites accessible to electromagnetic radiation, whether it is the bulk or the surface. As such, with chemisorption, one counts the sites available to catalysis. But chemical methods such as chemisorption of H_2 (or other gases) have limitations. The presence of metal-support interaction, formation of bulk hydrides, spillover effect, or contaminants can indeed alter the gas uptake. Difference between H_2-chemisorption analysis and XPS analysis can be attributed to differences in the surface analyzed by each technique. H_2-chemisorption analysis leads to higher estimation of mean particle sizes than XPS, indicating that XPS analysis (sampling depth of about 5 nm) may be able to detect some small ruthenium particles in deeper surface layers, which are not exposed for H_2-chemisorption, at the outermost surface.

In order to make an attempt to validate these techniques [18] a particular investigation was performed. Supported palladium nanoparticles with different diameters were synthesized by the water-in-oil microemulsion method using TiO_2 as support. The materials were characterized by all these techniques. It was concluded that XPS analysis could be a good and probably more accessible alternative to determine rapidly and with high accuracy nanosize particles of supported materials. It was showed the useful role of XPS in the analysis of small metallic particles. XPS analysis could be applied to highly dispersed particles which are not "visible" by the XRD method. It was also concluded that, in particular cases, XPS must be coupled with complementary methods such as XRD, gas chemisorption, or TEM.

In this study, catalysts were characterized by N_2 physisorption, XRD, X-ray photoelectron spectroscopy (XPS) and Transmission electron microscopy (TEM). For these reasons, XPS analysis, as a highly sensitive surface technique, has been principally used to determine with enough accuracy the dependence of the catalytic activity with the nanosize particles of Ru having a heterogeneous size distribution.

2. Material and methods

2.1. Synthesis of catalysts

2.1.1. Synthesis of colloidal suspensions of RuO_2 nanoparticles

Suspensions of RuO_2 nanoparticles were synthesized following the colloidal method [12–14]. Colloidal suspensions of RuO_2 nanoparticles were synthesized via slow hydrolysis/condensation of ruthenium chloride, by using H_2O_2 as oxidizing agent [17]. As hydrolysis proceeds, OH— ions and/or water molecules gradually replace the chloride ions from the inner coordination sphere of Ru, leading to ruthenium hydroxides and/or oxyhydroxides. The addition of hydrogen peroxide in the RuCl3 solution causes a fast oxidation of Ru(III) ions into Ru(IV). This increases the rate of the hydrolysis/condensation reactions, thus promoting the nucleation over the growth of particles. As a result, a highly dispersed hydrous RuO2 nanoparticles of (2 ± 0.2) nm is obtained, with interactions dominated by short-range forces, such as van der Waals attraction and surface charges.

An aqueous solution of ruthenium trichloride ($RuCl_3{}^*H_2O$ 99.99%, Alfa Aesar) and an aqueous solution of hydrogen peroxide (Acros Organics, 35 wt.% stabilized) were prepared. The H_2O_2 solution (13.513 vol.%) was slowly added into the ruthenium solution (0.11 M), under magnetic stirring (1500 rpm), allowing the oxidation of Ru(III) into Ru(IV). The final solution (0.0072 M in ruthenium) contained in a closed vessel was placed in a static oven at 95 °C for 2 h, and then it was cooled down to room temperature. Three suspensions were prepared containing the Ru mass required for Ru loadings of 3 wt.%, 5 wt.% and 7 wt.% in the final catalysts.

2.1.2. Synthesis of RuO_2/γ-Al_2O_3 catalysts

Catalysts were then synthesized via impregnation of alumina with RuO_2 colloids. Powdered γ-Al_2O_3 (Alfa Aesar, 99.97% (metals basis), $S_{BET} = 70\ m^2\ g^{-1}$) was added into each suspension, under vigorous stirring. Water was then evaporated, under reduced pressure at 50 °C, and the recovered sample was dried overnight in air at 110 °C. Then catalysts were calcined at 450 °C during 4 h. Three

catalysts containing 3 wt.%, 5 wt.% and 7 wt.% of Ru were prepared, denoted as $Ru3/Al_2O_3$, $Ru5/Al_2O_3$ and $Ru7/Al_2O_3$. In order to study reproducibility, each catalyst was prepared 3 times following the same procedure.

2.1.3. Preparation of mechanical mixtures

In order to have both small and larger Ru nanoparticles in close proximity, two mechanical mixtures containing (i) 50 wt.% $Ru3/Al_2O_3$ and 50 wt.% $Ru5/Al_2O_3$, and (ii) 50 wt.% $Ru3/Al_2O_3$ and 50 wt.% $Ru7/Al_2O_3$ were prepared. Both catalysts containing particles < 100 μm were dispersed in *n*-pentane (Merck, >98%) under vigorous stirring. The sample was recovered via slow evaporation of *n*-pentane, under stirring at 25 °C, and then it was dried overnight at 110 °C. The mixture was not further calcined and the final samples are denoted respectively as $Mix3+5/Al_2O_3$ and $Mix3+7/Al_2O_3$.

2.2. Catalytic activity measurements

Catalytic tests were carried out in a metallic fixed-bed tubular (8 mm I.D.) reactor, equipped with a frit to hold the catalyst and a K-type thermocouple to measure and control the temperature of the catalytic bed.

Three different tests were performed after reduction pretreatment of the catalysts: 1) Standard test, measuring the catalytic activity of ammonia synthesis; 2) Test under NH_3 + He treatment, following ammonia decomposition; 3) Test under NH_3 + He + H_2 treatment, following ammonia decomposition in presence of hydrogen. Standard test were additionally used to study the effect of the different treatments (NH_3 + He and NH_3 + He + H_2) on the catalytic activity of ammonia synthesis.

2.2.1. In situ reduction pretreatment

The catalyst (400 mg) previously sieved to a particle size range of 100–315 μm was reduced in pure H_2 (Praxair, 4.8) at 200 °C during 2 h (heating rate of 10 °C min^{-1}). The reactor was then cooled down to 50 °C.

2.2.2. Standard test (ST)

Temperature programmed tests were performed in the range 50–150 °C, in a flowing mixture (40 ml min^{-1}) of N_2/H_2 (1/3 vol.%), at 5 bar and a space velocity of 6000 ml h^{-1} $g_{cat}{}^{-1}$.

After fixing the reaction temperature and the flow of the gas mixture, steady state is rapidly reached, then the conversion and reaction rate are stable and remain unchanged during the whole duration of the test (1 h) at the fixed temperature (50 °C, 100 °C, 150 °C). Under the reaction conditions used, reaction rates of single catalysts and of their mechanical mixtures do not vary with time on stream.

Mass transfer limitations and diffusion rate-controlling regime were fully excluded for the conditions selected to perform catalytic tests, i.e. a flow rate of 40 ml min^{-1} and a particle size range of 100–315 μm. N_2 (Praxair, 5.0) and H_2(Praxair, 4.8) were used.

The effluents were analyzed online by using a gas chromatograph equipped with two thermal conductivity detectors. The sequence of analyses was performed in periods of 15 min, allowing the quantification of NH_3, H_2 and N_2.

The specific reaction rate r, considering a tubular packed bed reactor is given by

$$r = \frac{dX_A}{d\left(W/F_A\right)} \quad (1)$$

where X_A and F_A correspond to the conversion and the molar flow of reactant A, and W is the catalyst mass. The reactor was operated at differential conditions (X_A < 15%) at constant temperature. The forward rate of ammonia formation has been calculated as:

$$r_{forward} = \frac{F_{N_2,i}X_{N_2}}{W}\left(\frac{1}{1-\eta}\right) \quad (2)$$

where η is the approach to equilibrium factor and it corresponds to the $r_{backward}/r_{forward}$ ratio, as described elsewhere [12].

The turnover frequency (TOF) values have been calculated as:

$$TOF = \frac{r_{forward}}{D}\frac{M}{L} \quad (3)$$

where M and L correspond to the atomic mass of Ru and Ru loading (wt.%) in the catalyst. D is the dispersion of ruthenium, meaning the fraction of Ru surface atoms relative to the total Ru atoms present in the catalyst.

After the reaction of ammonia synthesis, the reverse reaction of NH_3 decomposition into N_2 and H_2 was studied under the same conditions and for the same catalysts. The effect of H_2 doping on the NH_3 decomposition was also studied.

In order to estimate the experimental error of the catalytic activity measurements, the following procedure was followed: i) $Ru3/Al_2O_3$, $Ru5/Al_2O_3$, and $Ru7/Al_2O_3$ single catalysts. and $Ru3/Al_2O_3$+$Ru5/Al_2O_3$ and $Ru3/Al_2O_3$+$Ru7/Al_2O_3$ mechanical mixtures were prepared, ii) 5 tests under standard test conditions were performed for each single catalysts and 2 test for the mixtures. Steady state measurements performed at each temperature were used to calculate the average nitrogen conversions, the average rate of NH_3 formation and theirrespective relative standard errors. The average standard error of the kinetic measurements was calculated from the errors obtained at the different temperatures. Results showed that the N_2 conversions and the rate of NH_3 formation are estimated with an error of less than 3 % .

2.2.3. Ammonia decomposition – test under NH_3 + He treatment (NH_3 test)

Catalysts were first reduced as indicated in Section 2.2.1. A flow (60 ml min^{-1}) of NH3 diluted in He (Praxair, NH3 5%vol.) was then injected to the reactor at 5 bar. The reactor temperature was maintained at 50 °C during 30 min, and then it was raised to 100 °C and 150 °C (heating rate of 5 °C min^{-1}), maintaining both temperatures for 45 min.

NH_3, H_2 and N_2 at the outlet gas were analyzed every 15 min, by gas chromatography. It is important to underline that the ammonia synthesis and ammonia decomposition are conducted under different flow conditions. The amount of ammonia sent to the reactor is several orders of magnitude greater than the ammonia synthesized during differential reactor condition tests. The reason for that was to obtain in a short time an answer of the influence of ammonia in the catalytic system.

2.2.4. Ammonia decomposition – test under NH_3 + He + H_2 treatment (NH_3 + H_2 test)

Catalysts were first reduced as indicated in Section 2.2.1. A flow of NH_3 diluted in He (60 ml min^{-1}) and a flow of pure H_2 (5 ml min^{-1}) were then injected to the reactor at 5 bar. Then, the same temperature-programmed test indicated in Section 2.2.3 was performed.

2.2.5. Effect of NH_3 on the catalytic activity of NH_3 synthesis (NH_3 test + ST)

Catalysts were reduced as indicated in Section 2.2.1. Then, a test was performed under a flow of NH_3 diluted in He (5%vol., 60 ml min^{-1}), at 5 bar, as described in Section 2.2.3. Afterwards, NH_3 flow is changed to pure He (100 ml min^{-1}), while the reactor is cooled down to room temperature and till no ammonia is observed

at the exit of the reactor (about one hour). Finally, the standard test (ST) is performed as described in Section 2.2.2.

2.2.6. Effect of $NH_3 + H_2$ on the catalytic activity of NH_3 synthesis ($NH_3 + H_2$ test + ST)

Catalysts were reduced as indicated in Section 2.2.1. Then, a test was performed under NH_3 diluted in He (5%vol., 60 ml min^{-1}) and a pure H_2 flow (5 ml min^{-1}), at 5 bar, as described in Section 2.2.2. Afterwards, $NH_3 + He + H_2$ flow is changed to pure He (100 ml min^{-1}), while the reactor is cooled down to room temperature and till no ammonia is observed at the exit of the reactor (about one hour). Finally, the standard test (ST) is performed as described in Section 2.2.2.

2.3. Physicochemical characterization

2.3.1. N_2 physisorption

N_2 (Praxair, 5.0) adsorption and desorption isotherms of the samples were recorded at 77 K (temperature of liquid N_2) using a Micromeritics Tristar 3000 apparatus. Samples were previously degassed overnight at 150 °C and 0.15 mbar. The specific surface area was calculated according to the BET method.

2.3.2. X-ray diffraction analysis

X-ray diffraction (XRD) spectra were recorded with a Bruker D8 X-ray diffractometer, operating in the reflection mode with a Cu Kα radiation (λ = 1.5406 Å and 1.5444 Å), at 40 kV and 40 mA. The data were collected in the 20–50° range (2θ) with steps of 0.02°.

The various compounds were identified by comparison of their profiles with the database JCPDS – International Center for Diffraction Data. X-ray diffraction line broadening analysis was used for characterizing supported Ru nanoparticles. The Scherrer formula was applied to estimate the average metal particle size. The X-ray pattern was fitted by least-squares fit assuming a Gaussian peak shape. The crystallite size (d_p) is calculated as a function of the peak width (B), the peak position ($2\theta_B$) and the wavelength of the incident X-ray beam (λ), according to the Scherrer's equation:

$$d_p = \frac{0.94\lambda}{B\cos\theta_B} \quad (4)$$

B is obtained as the full width at half maximum intensity (FWHM) of X-ray diffraction peak.

2.3.3. X-ray photoelectron spectroscopy

X-ray photoelectron spectra were obtained for calcined and tested samples with a SSI-X-probe (SSX-100/206) spectrometer equipped with a monochromatized microfocused Al K_α X-ray source, operating at 10 kV and 12 mA. After outgassing under vacuum (10^{-5} Torr) overnight, samples were placed in the analysis chamber where the residual pressure was of about 10^{-7} Torr. The charging effect was adjusted using flood gun energy at 8 eV and a fine-meshed nickel grid placed 3 mm above the sample surface. The pass energy was 150 eV and the spot size was 1000 μm. Angle between the normal to the sample surface and the direction of electron collection was 55°. The binding energy scale of the spectrometer was calibrated with respect to the Au $4f_{7/2}$ peak of gold, fixed at 83.98 eV, and the binding energies of O 1s, Al 2p, and Ru 3d were referenced to the C-(C,H) component of C 1 s band, fixed at 284.8 eV. In order to obtain the surface atomic concentrations, relative areas of corresponding peaks were normalized by using sensitivity factors based on the Scofield cross-sections. Peak decomposition was performed using the CasaXPS program (Casa Software, UK), assuming a 85/15 Gaussian/Lorentzian product function and a Shirley non-linear sigmoid-type baseline. As the Ru 3d core levels superimpose the C 1 s core level, a specific decomposition method was used using the CasaXPS program. After the subtraction of a non linear baseline (Shirley), the C 1 s – Ru 3d region were resolved with symmetric Gaussian-Lorenzian functions for the different chemical states of carbon together with tail-dampened Lorentzian asymmetric lineshapes for the ruthenium part of the signal. Metallic Ru was then represented with a characteristic doublet at 279.8 eV while the oxidized Ru species were described with the combination of a main doublet (280.7 eV) accompanied by a satellite doublet (282.6 eV). Each of them was simulated with a spin-orbit splitting of 4.17 eV and with the expected area ratio of 3:2. For the Ru 3p core levels, only the Ru $3p_{3/2}$ peak was fitted as it is common for well-separated doublets. Similar asymmetric line shapes where use to distinguish the metallic Ru part (461.2 eV) from the oxidized Ru part (main peak at 462.6 eV and its satellite at 465.5 eV). In both cases (Ru 3d and Ru $3p_{3/2}$), the oxidized part was computed as the sum of the main and satellite peaks.

Percentages of metallic Ru atoms were quantified in order to analyze changes in Ru oxidation state during the reduction and catalytic test. XPS analysis was not performed in situ. Indeed, after catalytic test, the sample was cooled down to room temperature under inert gas flow, so that any possible oxidation of the catalyst by exposure to air, during its transfer into XPS machine, is expected to be minor and would only concern the most external surface layer. Furthermore, XPS analysis might involve a mild reduction associated with the exposure to ultra-high vacuum conditions (10–5 Torr). Then, Ru atoms slightly oxidized under air, at the outermost layer, may be re-reduced at this stage.

Ru particle size was estimated from a model proposed by Kerkhof et al. [19], which considers cubic metallic crystallites of size, deposited over support sheets. Model predicts the average particle size from intensity ratio of monolayer and crystallite samples. This model depends strongly on the physical properties of the support and it seemed to be very sensitive to the small variation in the particle size distribution. The thickness (t) of these sheets is obtained from the support density and surface area, as shown below for alumina:

$$t = \frac{2}{\rho_{Al_2O_3} S_{BET,Al_2O_3}} \quad (5)$$

According to this model, the theoretical XPS $(Ru/Al)_m$ atomic ratio expected for a monolayer dispersion of ruthenium on alumina is given by:

$$\left(\frac{Ru}{Al}\right)_m = \left(\frac{Ru}{Al}\right)_b \frac{G(\varepsilon_{Ru})}{G(\varepsilon_{Al})} \frac{\sigma_{Ru}}{\sigma_{Al}} \frac{1}{2} \left(\frac{t}{\lambda_{Al-Al}}\right) \frac{1+\exp(-t/\lambda_{Ru-Al})}{1-\exp(-t/\lambda_{Ru-Al})} \quad (6)$$

where $(Ru/Al)_b$ is the bulk atomic ratio, calculated from the theoretical Ru content. G functions of the electron kinetic energies (ε) correspond to the spectrometer efficiencies and can be approximated as ε^{-1} σ_{Ru} and σ_{Al} are the relative photoelectron cross sections provided by Scofield [20]. λ_{Ru-Al} and λ_{Al-Al} correspond to the escape depths of Ru 3d3/2 and Al 2p photoelectrons through the alumina support, and were determined from the Tanuma et al. [21] algorithm, by using the QUASES-IMFP-TPP2M software [22].

In case of crystallite growth, the Ru particle size (C) was estimated from the XPS $(Ru/Al)_e$ experimental atomic ratio, by the following equation:

$$\frac{(Ru/Al)_e}{(Ru/Al)_m} = \frac{1-\exp\left(-C/\lambda_{Ru-Ru}\right)}{C/\lambda_{Ru-Ru}} \quad (7)$$

In the end, once the Ru particle size was estimated, the proportion of Ru located on the surface of the catalyst, compared to monolayer dispersion, was estimated. That corresponds to the Ru

Table 1
Ru particle size estimated by X-Ray diffraction analysis of fresh catalysts (single catalysts and mechanical mixtures), and after reduction and standard catalytic test (ST).

Catalysts	Particles diameter (nm)	
	Fresh	After reduction and standard test
$Ru3/Al_2O_3$	40.7	14.4
$Ru5/Al_2O_3$	46.7	18.5
$Ru7/Al_2O_3$	39.2	20.4
$Mix3+5/Al_2O_3$	40.1	18.7
$Mix3+7/Al_2O_3$	28.9	17.3

dispersion (%) in the catalyst, and is calculated with the following equation:

$$\textbf{\textit{Ru dispersion}} = 100\frac{6\,\boldsymbol{M_{Ru}}\,\boldsymbol{d_{Ru}}}{\boldsymbol{C}\,\boldsymbol{\rho_{Ru}}\,\boldsymbol{N_A}} \quad (8)$$

M_{Ru} the Ru molar mass ($g\,mol^{-1}$), d_{Ru} the Ru atomic density ($atom\,cm^{-2}$), ρ_{Ru} the Ru density ($g\,cm^{-3}$) and N_A the Avogadro's number.

2.3.4. Transmission electron microscopy (TEM)

TEM images of Ru nanoparticles supported on γ-Al_2O_3 were obtained with a FEI Tecnai 120 Twin microscope, operating at 120 kV and equipped with a Gatan Orius CCD numeric camera. The samples were prepared by ultrasonic dispersion of the powders in ethanol and a droplet of the dispersion was then placed onto a carboncoated copper grid. Some samples were selected for a high-resolution analysis (HRTEM) with a JEOL JEM 2010 microscope, operating at 200 kV and equipped with a Gatan camera. In this case, the samples were dispersed in water and deposited over commercial holey carbon-coated grids (200 mesh). Frequency histograms of Ru particle sizes, mean size and standard deviation were estimated considering more than 100 particle diameters measured on each sample. In order to fully appreciate the distribution of surface ruthenium atoms, the number of Ru particles from each size range of the histogram (ranges of 1 nm) was multiplied by the calculated surface of the particles (considering spherical particles), and then normalized.

3. Results

3.1. Characterization of fresh catalysts

3.1.1. X-ray diffraction

3.1.1.1. Single catalysts: $Ru3/Al_2O_3$, $Ru5/Al_2O_3$, and $Ru7/Al_2O_3$. Generally, the diffractograms have the same appearance and have the same peaks, regardless of the Ru loading of the catalysts (Fig. 1). For each of the three calcined catalysts, the presence of γ-Al_2O_3 alumina (JCPDS card 10-0425) and of RuO_2 ruthenium oxide (JCPDS card 40–1290) is clearly detected. The presence of metallic Ru (JCPDS card 6-0663) is not observed. Concerning the relative intensity of peaks, an increase of the two main peaks of RuO_2 (located at $2\theta = 28^\circ$ and $2\theta = 35^\circ$) is observed, compared to the main peak of γ-Al_2O_3 ($2\theta = 46^\circ$), which corresponds to the increase of Ru content in the catalysts. The peak used to estimate the particle size is the one assigned to RuO_2, at $2\theta = 28^\circ$. The mean sizes of RuO_2 supported particles estimated for fresh catalysts are shown in Table 1. The mean RuO_2 size is similar for all single catalysts (around 40 nm), regardless of the Ru loading.

3.1.1.2. Mechanical mixtures. The observations are mostly the same for mechanical mixtures and single catalysts (Table 1). Indeed, for mixtures, the XRD pattern and peak position are similar. The presence of γ-Al_2O_3 alumina and RuO_2 oxide is detected, but no trace of metallic Ru is observed. The relative intensity of the main RuO_2 peak, compared to the main γ-Al_2O_3 peak, is higher for the $Mix3+7/Al_2O_3$, which is in agreement with the highest Ru content in this mixture. The mean size of RuO_2 particles in $Mix3+5/Al_2O_3$ is the same than in both single catalysts constituting that mixture, while the mean RuO_2 size in $Mix3+7/Al_2O_3$ is about 20% lower than in non-mixed catalysts.

3.1.2. X-ray photoelectron spectroscopy

3.1.2.1. Single catalysts: $Ru3/Al_2O_3$, $Ru5/Al_2O_3$, and $Ru7/Al_2O_3$. Results of the analyses of fresh catalysts are shown in Table 2. The mean RuO_2 particles size range from 3.7 to 9.1 nm and Ru dispersion from 18% to 7% for samples $Ru3/Al_2O_3$, $Ru5/Al_2O_3$ and $Ru7/Al_2O_3$ respectively. This confirms that the selected colloidal method leads to RuO_2 particles of nanometric size, and they are deposited on alumina through a mechanism allowing certain growth of supported particles as the Ru content increases. Accordingly, Ru dispersion decreases as the Ru loading increases. Binding energy of around 74.4 eV was obtained for Al2p photoelectrons, indicating the presence of non-modified γ-Al_2O_3 support, and it is about the same for all fresh samples. Binding energy of Ru3p3/2 (462.5 eV) is nearly the same for all fresh samples, indicating the presence of RuO_2.

There is no indication of traces of Cl in the fresh catalysts. In order to obtain the atomic concentrations of oxygen, ruthenium, aluminum and carbon at the surface of each sample, O 1s, Ru 3d, Al 2p and C 1s peaks were used, respectively. Surface atomic concentrations of both oxygen and aluminum are identical in all catalysts, and they are in a ratio of 3:2. The surface carbon concentration is similar (between 7.8% and 9.9%) in all single catalysts ($Ru3/Al_2O_3$, $Ru5/Al_2O_3$, and $Ru7/Al_2O_3$), and between 6.6% and 7.7% in the mixtures.

The experimental XPS (Ru/Al) atomic ratio is similar in all single catalysts (about 0.011), regardless of the Ru loading. These values are lower than the theoretical atomic ratios calculated for a RuO_2 monolayer (from 0.017, for 3 wt.% Ru, to 0.042, for 7 wt.% Ru), that is, considering that all Ru atoms are forming part of only one RuO_2 layer over alumina surface.

3.1.2.2. Mechanical mixtures. Results are presented in Table 2. In the case of mixtures, the $(Ru/Al)_{exp}$ atomic ratio is far below the value predicted for a monolayer of RuO_2 on alumina surface. The same surface atomic concentration of Ru is observed for all catalysts, mixed or not. The XPS $(Ru/Al)_{exp}$ atomic ratio for the fresh mixtures is about the average of the values of the parent catalysts suggesting that the fresh mixtures of separated catalysts ($Ru3/Al_2O_3 + Ru5/Al_2O_3$ and $Ru3/Al_2O_3 + Ru7/Al_2O_3$) have been made without any modification of the separately prepared catalysts.

3.1.3. Nitrogen physisorption

For all types of catalysts (single and mechanical mixtures) except the $Ru3/Al_2O_3$, specific surface area (BET) is similar and is about 65 m^2/g. The surface area of the 3 wt.% Ru catalyst is slightly higher (80 m^2/g) than the others.

3.2. Catalytic activity in ammonia synthesis – standard test (ST)

The conversion of nitrogen, the rate of ammonia formation (in $\mu mol_{NH3}/s\,g_{cata}$) and the turnover frequency (TOF) obtained at 100 °C and 150 °C are presented in Table 3. No catalytic activity is observed at 50 °C.

3.2.1. Influence of Ru loading and temperature

3.2.1.1. Single catalysts: $Ru3/Al_2O_3$, $Ru5/Al_2O_3$, and $Ru7/Al_2O_3$. In Fig. 2, TOF in ammonia synthesis obtained in ST, is plotted as a

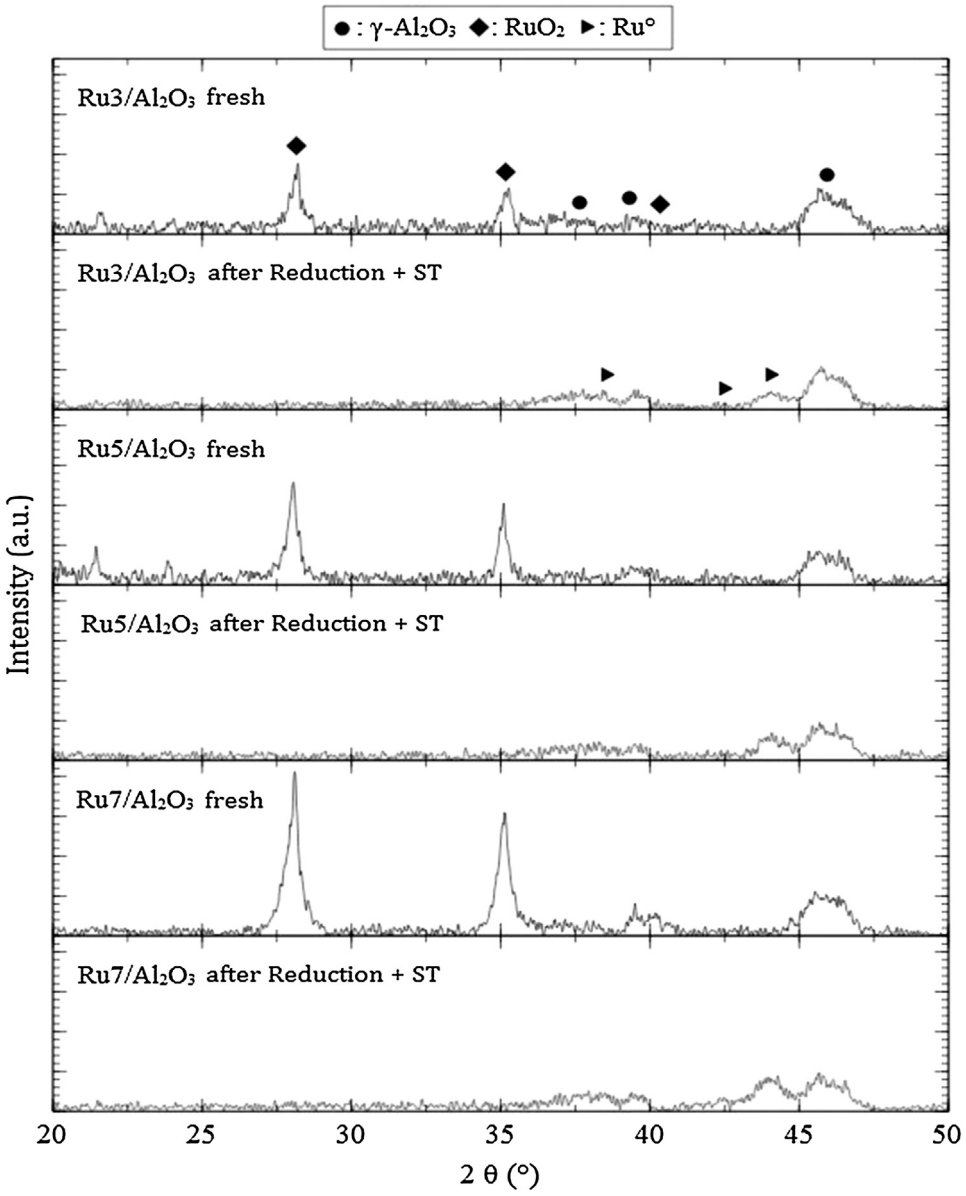

Fig. 1. XRD patterns of fresh $Ru3/Al_2O_3$, $Ru5/Al_2O_3$ and $Ru7/Al_2O_3$ single catalysts and after reduction and standard test 5ST).

Table 2
XPS atomic concentrations (O, C, Ru, and Al), (Ru/Al) atomic ratios (experimental and for a theoretical monolayer), average Ru particle size and Ru dispersion, for fresh single catalysts and mechanical mixtures.

Catalysts	Atomic concentration (%)				(Ru/Al) atomic ratio		Average Ru particle size (nm)	Ru dispersion (%)
	O	C	Ru	Al	$(Ru/Al)_{exp}$	$(Ru/Al)_{monolayer}$		
$Ru3/Al_2O_3$	55.3	9.9	0.4	34.4	0.011	0.017	3.7	18
$Ru5/Al_2O_3$	55.7	8.2	0.4	35.8	0.010	0.029	6.9	9
$Ru7/Al_2O_3$	55.6	7.8	0.4	36.2	0.011	0.042	9.1	7
$Mix3+5/Al_2O_3$	55.6	7.7	0.4	36.3	0.012	0.023	–	–
$Mix3+7/Al_2O_3$	56.5	6.6	0.4	36.5	0.011	0.029	–	–

Table 3
Catalytic performance of single catalysts and mechanical mixtures in ammonia synthesis standard test (ST), without NH_3 pretreatment. Experimental error <3%.

Catalysts	N_2 Conversion (%)		Rate of NH_3 formation ($\mu mol_{NH3}\ s^{-1}\ g_{cat}^{-1}$)		TOF ($10^{-2}\ s^{-1}$)	
	100 °C	150 °C	100 °C	150 °C	100 °C	150 °C
$Ru3/Al_2O_3$	6.6	5.8	1.22	1.08	2.3	2.0
$Ru5/Al_2O_3$	6.7	6.5	1.24	1.20	2.8	2.7
$Ru7/Al_2O_3$	6.0	6.1	1.10	1.12	2.3	2.4
$Mix3+5/Al_2O_3$	8.5	11.1	1.58	2.06		
$Mix3+7/Al_2O_3$	10.2	11.5	1.90	2.13		

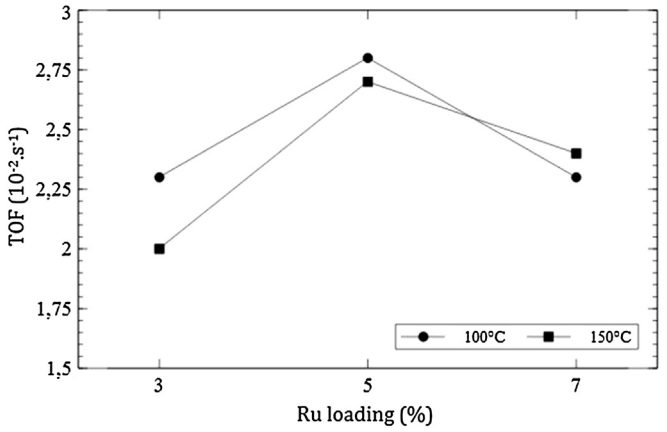

Fig. 2. Catalytic activity of ammonia synthesis (TOF values) as a function of the Ru loading in single catalysts, at 100 °C and 150 °C. Experimental error <3%.

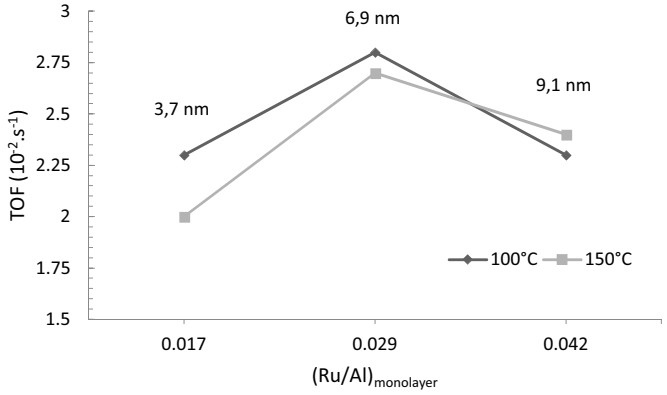

Fig. 3. Catalytic activity of ammonia synthesis (TOF values) as a function of the XPS (Ru/Al) monolayer of $Ru3/Al_2O_3$, $Ru5/Al_2O_3$ and $Ru7/Al_2O_3$ single catalysts at 100 °C and 150 °C. The size of Ru nanoparticle is also indicated. Experimental error <3%.

function of Ru loading. At both temperatures, the highest TOF is observed for the catalyst containing 5% of Ru.

No activity is detected at 50 °C. Between 100 °C and 150 °C, TOF value and nitrogen conversion slightly decrease for $Ru3/Al_2O_3$ catalyst, while they remain almost the same for $Ru5/Al_2O_3$ and $Ru7/Al_2O_3$ catalysts, as shown in Fig. 2 and Table 3 (ST).

Similar results are observed in Fig. 3, where TOF in ammonia synthesis is plotted as a function of dispersion given by the XPS $(Ru/Al)_{monolayer}$ ratio. The TOF is proportional to the dispersion of the metallic surface of Ru atoms given by XPS. In addition, in order to emphasize the role of the size of Ru nanoparticles, we have added in the same Fig. 3, the mean size of Ru of each sample. The role of the mean size of Ru nanoparticles is clearly put in evidence.

3.2.1.2. Mechanical mixtures. The nitrogen conversion obtained for the mixtures $Mix3+5/Al_2O_3$ and $Mix3+7/Al_2O_3$ is plotted in Fig. 4 as a function of the reaction temperature, along with the theoretical conversions calculated directly from the contribution of the two single catalysts (50% each) constituting the mixtures. No activity was detected at 50 °C.

Nitrogen conversions obtained for both mechanical mixtures, at 100 °C and 150 °C, are higher than the theoretical conversions, which indicate a synergy in the catalytic activity of the mixtures. For both mixtures, the reaction rate is even higher than the highest rate presented by the single catalysts constituting the mixture (Table 3). There is indeed a positive effect of mixing the catalysts on their catalytic activity. The activity of $Mix3+7/Al_2O_3$ is higher than the activity of $Mix3+5/Al_2O_3$, and the difference is more important at 100 °C. At 150 °C, the catalytic performances are mostly the same. Therefore, the catalytic activity of a mixture might depend on the Ru loading and Ru particle sizes of catalysts constituting the mixture. The reaction temperature has also an effect on the catalytic performance of mixtures. In fact, the activity of single catalysts remains unchanged from 100 °C and 150 °C (Fig. 2), while the activity of mixtures is much higher at 150 °C than at 100 °C.

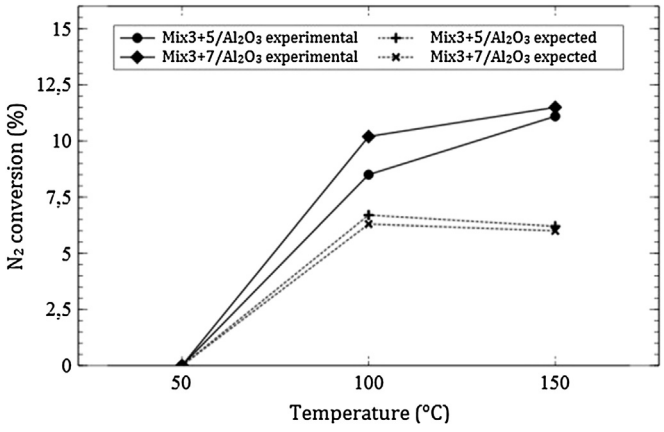

Fig. 4. Catalytic activity. N_2 conversion as a function of the temperature, for mechanical mixtures. The expected activity is plotted in dashed line, corresponding to the average of the N_2 conversions obtained, separately, for the two catalysts constituting the mixture. Experimental error <3%.

3.3. Characterization of catalysts after reduction and standard test

3.3.1. X-ray diffraction

3.3.1.1. Single catalysts: $Ru3/Al_2O_3$, $Ru5/Al_2O_3$, and $Ru7/Al_2O_3$. The RuO_2 peak, clearly detected for the fresh calcined catalysts, is no longer detected after reduction and standard catalytic test of ammonia synthesis (ST), and the peak corresponding to metallic Ru appears instead. After reduction and standard test, the relative intensity of the main metal Ru peak ($2\theta = 44°$), compared to the main γ-alumina peak ($2\theta = 46°$), increases with the Ru loading (Fig. 1).

The mean sizes of supported Ru particles estimated after reduction and standard test are presented in Table 1, along with the values corresponding to fresh catalysts. The peak at $2\theta = 44°$, assigned to metallic Ru, is used for the particle size estimation. In reduced and tested catalysts, the size estimated for Ru particles is significantly lower (50 to 60%) than in fresh catalyst, for all Ru loadings. Clearly, RuO_2 particles are larger than metallic Ru particles.

3.3.1.2. Mechanical mixtures. Changes in the diffratogram of mixtures, after being reduced and exposed to the standard catalytic test, are similar than those observed for single catalysts. Indeed, metallic Ru peaks also appear replacing RuO_2 peaks.

Ru particle sizes estimated after reduction and standard test are shown in Table 1, along with values obtained for the corresponding fresh catalysts. The metallic Ru peak at $2\theta = 44°$ is used for the estimation. Ru particles in reduced and tested catalysts are 40–50% smaller than RuO_2 particles in fresh catalysts.

3.3.2. X-ray photoelectron spectroscopy

3.3.2.1. Single catalysts: $Ru3/Al_2O_3$, $Ru5/Al_2O_3$, and $Ru7/Al_2O_3$. The XPS results obtained for fresh catalysts and the catalysts exposed to reduction and standard catalytic test are given in Table 2 and in Fig. 5. For all single catalysts, oxygen and carbon atomic concentrations are the same before and after reduction and standard test

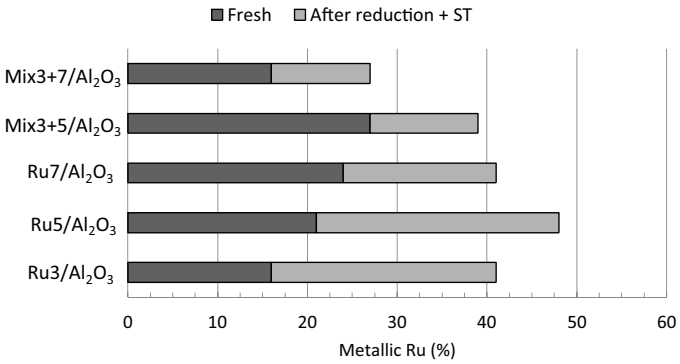

Fig. 5. Percentage of metallic Ru obtained by XPS analysis of fresh catalysts (single catalysts and mixtures), and after reduction and standard catalytic test (ST).

Table 4
XPS atomic concentrations (O, C, Ru, and Al) and (Ru/Al) atomic ratios, for single catalysts and mechanical mixtures after reduction and standard test.

Catalysts	Atomic concentration (%)				(Ru/Al)exp atomic ratio
	O	C	Ru	Al	
$Ru3/Al_2O_3$	56.8	10.9	0.5	31.8	0.015
$Ru5/Al_2O_3$	55.1	8.1	0.6	36.2	0.017
$Ru7/Al_2O_3$	55.5	7.5	0.6	36.5	0.016
$Mix3+5/Al_2O_3$	55.6	6.6	0.3	37.5	0.008
$Mix3+7/Al_2O_3$	55.6	7.4	0.3	36.7	0.009

(Table 4). Binding energy of Ru3p3/2 (462.5 eV) is nearly the same for all fresh samples, indicating the presence of RuO_2. A decrease of about 2 eV is observed after reduction and catalytic test. XPS also reveals the presence of remaining reduced Ru in all fresh calcined catalysts (Fig. 5). The percentage of metallic Ru from the total surface Ru atoms detected by XPS in the calcined catalysts, increases with the Ru loading.

For the fresh catalyst the XPS $(Ru/Al)_{exp}$ atomic ratios are nearly the same (Table 2). However the XPS $(Ru/Al)_{monolayer}$ atomic ratio increases with the Ru loading (from 0.017 to 0.042), indicating that the surface of the support is more covered by Ru nanoparticles when the Ru loading increases. After reduction and standard test, the XPS $(Ru/Al)_{exp}$ atomic ratio increases by about 50% (from about 0.010 to about 0.015, indicating that after these two events there is an enrichment of the surface in Ru. This enrichment in Ru is due to the reduction of Ru (Table 4). The Ru particles size range from 3.7 to 9.1 nm and Ru dispersion from 18% to 7% for samples $Ru3/Al_2O_3$, $Ru5/Al_2O_3$ and $Ru7/Al_2O_3$ respectively (Table 2).

3.3.2.2. Mechanical mixtures. Binding energies of Ru3p3/2 photoelectrons decrease in about 2 eV, indicating that Ru is reduced after reduction treatement and catalytic test. As in the case of single catalysts, the XPS analysis reveals the presence of metallic Ru in the fresh catalysts (Fig. 3). The percentage of surface Ru atoms that remain reduced after calcination is higher in the $Mix3+5/Al_2O_3$ fresh sample. The increase of Ru metallic percentage during the reduction step and the standard test is similar (about 12%) in both mixtures.

The XPS $(Ru/Al)_{exp}$ atomic ratio for the mixtures ($Ru3/Al_2O_3 + Ru5/Al_2O_3$ and $Ru3/Al_2O_3 + Ru7/Al_2O_3$) after reduction and standard test the are lower compared to the values of the parent catalysts.

3.3.3. TEM analysis

In Fig. 6 is presented TEM image of Ru nanoparticles in $Ru3/Al_2O_3$ and $Ru7/Al_2O_3$ catalysts prepared by colloidal method, after catalytic test at 100 °C, 5 bar and the particle size distribution. Samples prepared by colloidal method contain well-defined round Ru nanoparticles with a narrower size distribution (standard deviation of 0.9 nm). As shown by TEM images of $Ru3/Al_2O_3$ and $Ru7/Al_2O_3$ tested catalysts, most particles are well separated and do not form large agglomerates. For $Ru3/Al_2O_3$ it is observed particles in the range 3–6 nm. For $Ru7/Al_2O_3$ it is observed particles in the range 2–5 nm. Ru particles in $Ru7/Al_2O_3$ catalyst present a mean size of 3.6 nm (S.D. ± 0.9 nm), whereas the mean Ru particle size in the $Ru3/Al_2O_3$ catalyst is 4.8 nm (S.D. ± 0.9 nm). In Fig. 7 is presented the TEM image of a supported Ru particle in $Ru3/Al_2O_3$

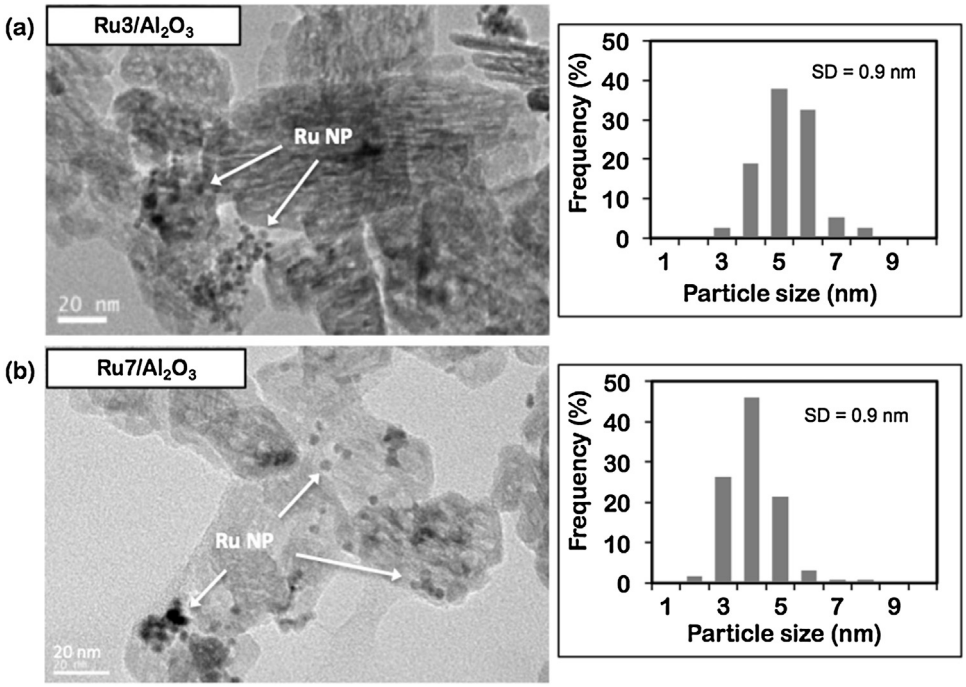

Fig. 6. TEM image of Ru nanoparticles in catalysts prepared by colloidal method, after catalytic test at 100 °C, 5 bar and particles size distribution.

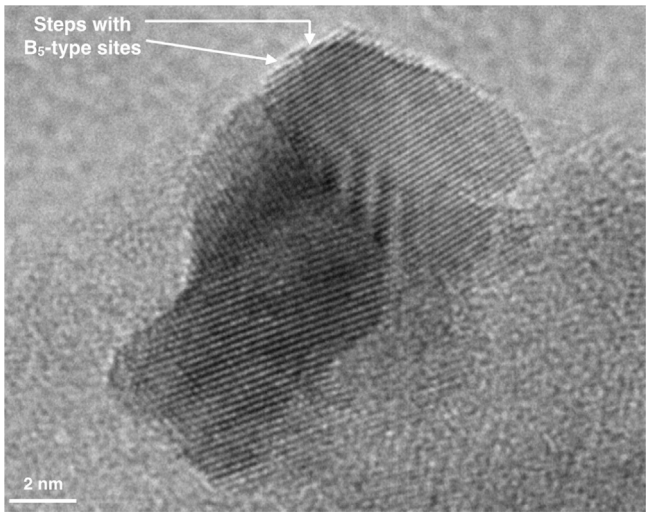

Fig. 7. TEM image of a supported Ru particle in $Ru3/Al_2O_3$ tested catalyst, exhibiting stepped surfaces where the formation of B_5-type sites is expected.

tested catalyst, exhibiting stepped surfaces where the formation of B_5-type sites is expected.

3.3.4. Nitrogen physisorption

3.3.4.1. Single catalysts: $Ru3/Al_2O_3$, $Ru5/Al_2O_3$, and $Ru7/Al_2O_3$. For Ru loadings of 3 wt.% and 5 wt.%, a decrease of the specific surface area is observed (from 80 to 67 m^2/g and from 67 to 40 m^2/g, respectively). Meanwhile, the specific surface area of the catalyst containing 7 wt.% of Ru remains unchanged (about 66 m^2/g).

3.3.4.2. Mechanical mixtures. The specific surface area of mixtures slightly changes as a result of the reduction and standard test (from 64 to 68 m^2/g, for Mix3 + 5/Al_2O_3, and from 65 to 62 m^2/g, for Mix3 + 7/Al_2O_3).

3.4. Tests under NH_3+He treatment (NH_3 test)

The decomposition of ammonia was tested under the same temperature and pressure conditions used for ammonia synthesis. Ammonia was introduced in the reactor as a single reagent, in presence of the same catalysts used for the standard tests (Sections 2.2.3 and 2.2.4). Ammonia decomposition was qualitatively analyzed via gas chromatography, following H_2 and N_2 formation. Although H_2 and N_2 concentrations reached in the tests were below the respective quantification limits, some relevant qualitative information is obtained. At all temperatures (50, 100 and 150 °C), hydrogen and nitrogen are produced in presence of $Ru3/Al_2O_3$, $Ru5/Al_2O_3$ and $Ru7/Al_2O_3$ single catalysts. Nitrogen concentration seems to be higher at 150 °C.

3.5. Test under NH_3 + He + H_2 treatment (NH_3 + H_2 test)

The main observations are the presence of a large H_2 peak (as a result of the addition of hydrogen to the inlet gas flow) and the absence of a N_2 peak. These observations are the same for all single catalysts.

3.6. Study of NH_3 effect on the catalytic activity of NH_3 synthesis

3.6.1. Single catalysts: $Ru3/Al_2O_3$, $Ru5/Al_2O_3$ and $Ru7/Al_2O_3$

The catalytic activities measured during ammonia synthesis, after the different pretreatments, are shown in Table 5 (reaction rate) and Fig. 8 (nitrogen conversion). The results obtained in standard tests (ST) are compared with those obtained in standard tests preceded by NH_3+He treatment (NH_3 Test + ST) and in standard tests preceded by NH_3 + He + H_2 treatment (NH_3 + H_2 Test + ST).

3.6.1.1. Effect of NH_3 pretreatment. N_2 conversions obtained during the standard test preceded by NH_3+He treatment of single catalysts are presented in Fig. 8, at 100 °C and 150 °C. The catalytic activity of NH_3 synthesis, decreases after exposing the catalyst to NH_3+He treatment. A similar decrease in N_2 conversion, in the range of 20–35%, is observed at both temperatures and for all the catalysts. This is more clearly observed when N_2 conversion is plotted as a function of the Ru loading (Fig. 9).

In conclusion, pretreating the catalysts with NH_3 has an inhibitory effect on their performance during NH_3 synthesis, which does not significantly depend on the Ru loading or the reaction temperature.

3.6.1.2. Influence of H_2 on NH_3 inhibitory. N_2 conversions obtained during the standard test preceded by NH_3 + He + H_2 treatment of single catalysts is plotted in Fig. 10 as a function of the Ru loading, at 100 °C and 150 °C. These results are compared with those obtained in standard tests (ST) and in standard tests preceded by NH_3 + He treatment (in absence of hydrogen).

The pretreatment in presence of hydrogen (NH_3+He+H_2) leads to higher N_2 conversions than the pretreatment in absence of hydrogen (NH_3+He), although N_2 conversions are still lower than for standard tests without NH_3 pretreatment. That is, the inhibitory effect of NH_3 is lower when the catalyst is pretreated in presence of hydrogen. Moreover, the role of H_2 in lowering the NH_3

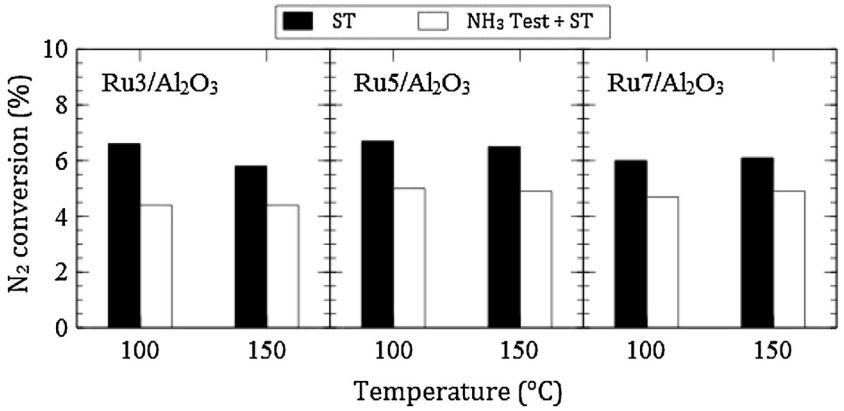

Fig. 8. Catalytic activity. N_2 conversion of single catalysts as a function of temperature, during standard tests without NH_3 pretreatment (ST), and after NH_3 treatment in absence of hydrogen (NH_3 Test + ST). Experimental error <3%.

Table 5
Rate of NH_3 formation with single catalysts, during standard tests without NH_3 pretreatment (ST), and after NH_3 treatments in absence and presence of hydrogen (NH_3 Test + ST and $NH_3 + H_2$ Test + ST, respectively). Experimental error <3%.

Catalysts	Rate of NH_3 formation ($\mu mol_{NH3}\ s^{-1}\ g_{cat}^{-1}$)					
	ST		NH_3 Test + ST		$NH_3 + H_2$ Test + ST	
	100 °C	150 °C	100 °C	150 °C	100 °C	150 °C
$Ru3/Al_2O_3$	1.22	1.08	0.81	0.82	1.10	1.08
$Ru5/Al_2O_3$	1.24	1.20	0.93	0.90	1.09	1.17
$Ru7/Al_2O_3$	1.10	1.12	0.88	0.91	1.00	1.09

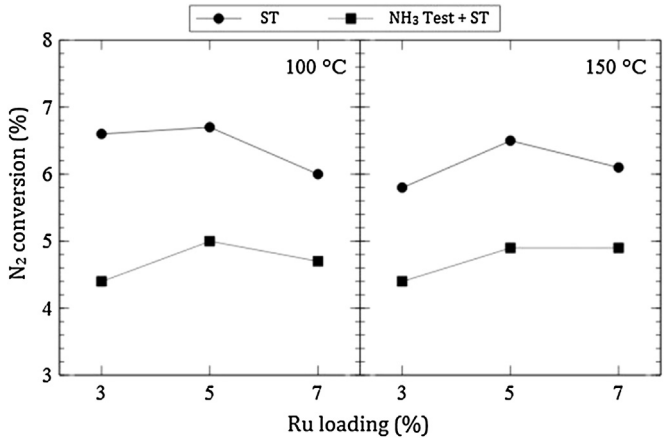

Fig. 9. Catalytic activity. N_2 conversion of single catalysts as a function of Ru loading, during standard tests without NH_3 pretreatment (ST), and after NH_3 treatment in absence of hydrogen (NH_3 Test + ST). Experimental error <3%.

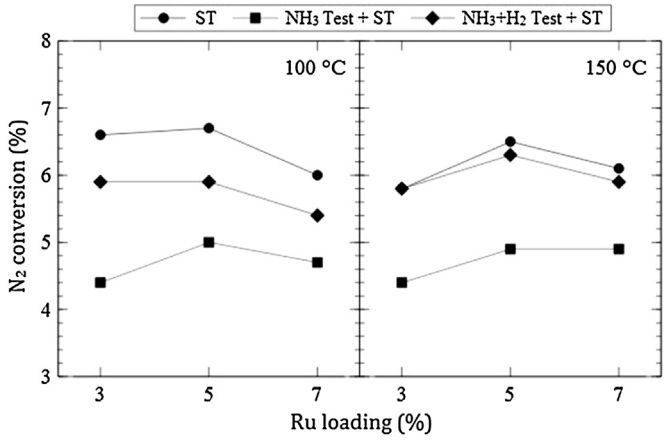

Fig. 10. Catalytic activity. N_2 conversion of single catalysts as a function of Ru loading, during standard tests without NH_3 pretreatment (ST), and after NH_3 treatments in absence and presence of hydrogen (NH_3 Test + ST and $NH_3 + H_2$ Test + ST, respectively). Experimental error <3%.

inhibitory effect is more important at 150 °C than at 100 °C. In fact, after NH_3+He+H_2 pretreatment, N_2 conversions measured during ammonia synthesis at 150 °C are very similar to the conversions obtained in the standard tests without NH_3 pretreatment.

3.6.2. Mechanical mixtures: mix3+5/Al_2O_3 and Mix3+7/Al_2O_3

3.6.2.1. Effects of the presence of NH_3. The catalyst mixtures have showed better catalytic activity than the conventional catalysts, the inhibitory effect of NH_3 has been studied in their presence, and the influence of H_2 on this inhibitory effect.

Fig. 11 shows N_2 conversions obtained for standard tests with mechanical mixtures, which were exposed to different pretreatments. The decrease in the catalytic activity after NH_3+He treatment is more significant in the case of mixtures than for single catalysts. Besides, the NH_3 inhibitory effect on the activity of mixtures (Table 6) is more important at 150 °C than at 100 °C. Indeed, the catalytic activity of both mixtures drops in about 50%, at 100 °C, and in about 70%, at 150 °C. The N_2 conversion achieved after NH_3+He pretreatment turns out being around 4%, in all cases.

The catalytic activity increases again when performing the NH_3+He pretreatment in presence of H_2, and the measured N_2 conversions are similar to the ones obtained for standard tests without NH_3 pretreatment. In most of the cases, the activity is not fully recovered, while in the case of Mix3+5/Al_2O_3 at 100 °C, N_2 conversion reaches back the same value obtained in the original standard test.

3.7. Characterization of catalysts after different pretreatments and standard tests

3.7.1. X-ray diffraction of single catalysts

Results are similar for all single catalysts. After NH_3+He pretreatment (NH_3 Test + ST) or NH_3+He+H_2 pretreatment (NH_3+H_2 Test + ST) of reduced catalysts, followed by a standard test, RuO_2 peaks is no longer appear in the diffractograms, and only metallic Ru is observed. It is nevertheless possible to distinguish that the relative intensity of the metallic Ru peak at $2\theta = 44°$, compared to the γ-alumina peak at $2\theta = 46°$, in catalysts pretreated with NH_3+He+H_2 is higher than for other pretreatments. Concerning γ-Al_2O_3, the intensity of the peak at $2\theta = 46°$ is the same for all single catalysts, indicating that the support is not affected by any treatment.

3.7.2. X-ray photoelectron spectroscopy

3.7.2.1. Single catalysts: Ru3/Al_2O_3, Ru5/Al_2O_3 and Ru7/Al_2O_3. Fig. 12 shows the surface percentage of metallic Ru in the fresh catalysts, and the catalysts reduced and exposed to standard tests preceded by NH_3+He treatment (NH_3 Test + ST) or NH_3+He+H_2 treatment ($NH_3 + H_2$ Test + ST). In most of the cases, the percentage of metallic Ru significantly increases after the reduction, pretreatment and subsequent standard test, as compared to the fresh calcined samples. The percentage of metallic Ru decreases when the catalyst is exposed to NH_3 Test + ST, compared to the Ru^0 percentage reached after reduction and standard test (without NH_3 pretreatment), and it significantly increases when the pretreatment is performed in presence of hydrogen (NH_3+He+H_2). Ru5/Al_2O_3 catalyst exhibits the most significant decrease in Ru^0 percentage due to the NH_3+He pretreatment. The highest percentage of metallic Ru is observed for the reduced Ru7/Al_2O_3 catalyst, after being exposed to NH_3+He+H_2 treatment and the standard test.

3.7.2.2. Mechanical mixtures. The percentage of metallic Ru in the fresh mixtures (Mix3 + 5/Al_2O_3 and Mix3 + 7/Al_2O_3), and the mixtures after reduction, pretreatment and standard test (ST, NH_3 Test + ST and NH_3+H_2 Test + ST) are shown in Fig. 13. The percentage of metallic Ru in the mixtures increases in about 12% after reduction and standard test. In the case of Mix3 + 5/Al_2O_3, the Ru^0 percentage after reduction, NH_3 + He treatment and standard test remains almost the same than in the fresh mixture, while it slightly

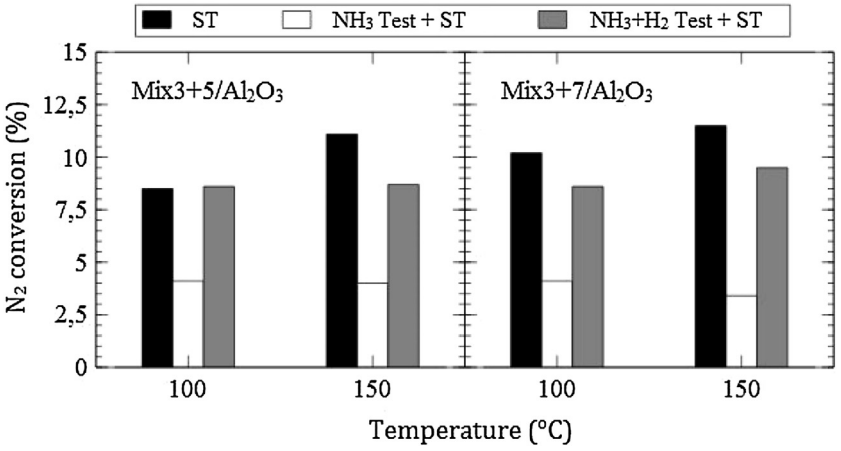

Fig. 11. Catalytic activity. N_2 conversion of mechanical mixtures as a function of temperature, during standard tests without NH_3 pretreatment (ST), and after NH_3 treatments in absence and presence of hydrogen (NH_3 Test + ST and $NH_3 + H_2$ Test + ST, respectively). Experimental error <3%.

Table 6
Rate of NH_3 formation with mechanical mixtures, during standard tests without NH_3 pretreatment (ST), and after NH_3 treatments in presence or absence of hydrogen. Experimental error <3%.

Catalysts	Rate of NH_3 formation ($\mu mol_{NH3}\ s^{-1}\ g_{cat}^{-1}$)					
	ST		NH_3 Test + ST		$NH_3 + H_2$ Test + ST	
	100 °C	150 °C	100 °C	150 °C	100 °C	150 °C
Mix3 + 5/Al_2O_3	1.58	2.06	0.77	0.74	1.59	1.62
Mix3 + 7/Al_2O_3	1.90	2.13	0.75	0.64	1.58	1.77

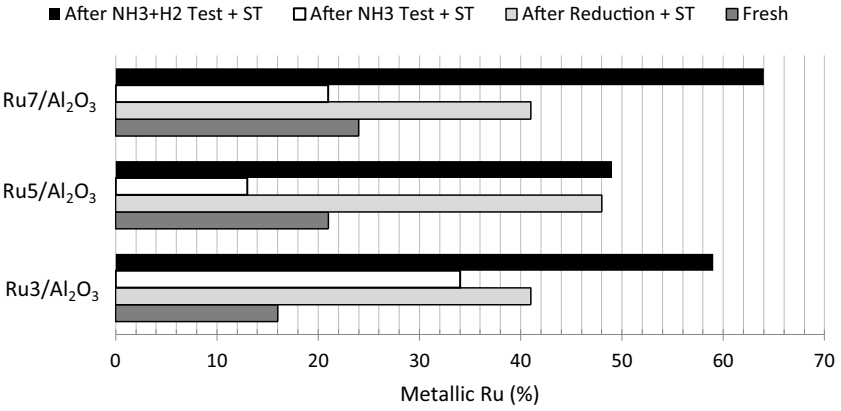

Fig. 12. Percentage of metallic Ru obtained by XPS analysis of fresh single catalysts, and after reduction and standard catalytic tests (ST) preceded by different pretreatments.

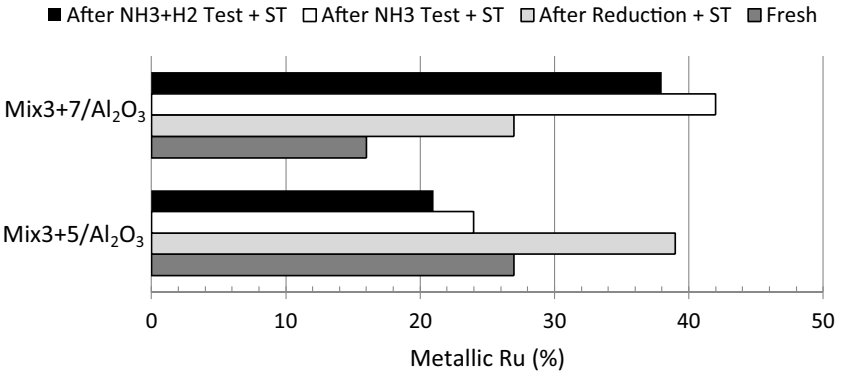

Fig. 13. Percentage of metallic Ru obtained by XPS analysis of fresh mechanical mixtures, and after reduction and standard catalytic tests (ST) proceeded by different pretreatments.

decreases after reduction, $NH_3 + He + H_2$ treatment and standard test. On the contrary, the percentage of metallic Ru in the fresh $Mix3 + 7/Al_2O_3$ mixture significantly increases during the reduction and standard test preceded by the NH_3 treatment, either in presence or absence of hydrogen.

4. Discussion

4.1. Single catalysts: $Ru3/Al_2O_3$, $Ru5/Al_2O_3$ and $Ru7/Al_2O_3$

4.1.1. State of catalysts and standard catalytic test (ST)

Ru loading has an influence on the textural and structural characteristics of catalysts. $Ru3/Al_2O_3$ catalyst presents the higher specific surface area. Al_2O_3 support remains unchanged in all catalysts. Ru particle sizes obtained by XRD analysis are similar for all Ru loadings (about 40 nm, Scherrer's equation), and much higher than those estimated by XPS analysis, which instead increase with the Ru loading, (3.7, 6.9 and 9.1 nm for $Ru3/Al_2O_3$, $Ru5/Al_2O_3$ and $Ru7/Al_2O_3$, respectively). As discussed above, because of the presence of very small nanoparticles in most catalysts, X-ray diffraction analysis does not give a reliable estimation of particle sizes. Indeed, mostly large crystals are detected by XRD, which leads to an overestimation of the mean particle size. In agreement with the increasing particle size, the dispersion of Ru decreases with the Ru loading, and therefore, $Ru3/Al_2O_3$ exhibits the highest fraction of surface Ru atoms. While only RuO_2 is detected by XRD analysis of fresh samples, the XPS analysis shows that a certain percentage of Ru at the catalyst surface remains in a reduced state after calcination. An important part of RuO_2 is reduced during the reduction pretreatment and catalytic test, leading to an increase in the fraction of metallic Ru, which depends on the Ru loading of the catalyst.

The reaction temperature influences the catalytic activity of ammonia synthesis. In spite that the reaction is thermodynamically possible at low temperatures, no detectable catalytic activity occurs at 50 °C. The maximum catalytic activity is reached with $Ru5/Al_2O_3$ catalyst, at 100 °C. The rate of ammonia formation decreases for temperatures over 100 °C, revealing a change in the apparent activation energy. This behaviour could be assigned to ammonia adsorption and dissociation on Ru particles (via reverse reaction) or to an inhibitory effect of ammonia adsorption on the support. The size of Ru nanoparticles influences their catalytic performance in ammonia synthesis. The higher catalytic activity was not obtained for the highest mean size of Ru nanoparticles, but for a mean size of 6.9 nm, corresponding to the catalyst with 5 wt.% of Ru. This is in agreement with previous findings indicating that the activity of ammonia synthesis increases with the mean size of Ru particles in the range 2–7 nm, and the highest activity is reached for a broad size distribution of Ru nanoparticles, including small and large nanoparticles. Interestingly, $Ru3/Al_2O_3$ and $Ru7/Al_2O_3$ catalysts, having different XPS mean sizes of Ru particles (3.7 nm and 9.1 nm, respectively), led to the same TOF value at 100 °C ($2.3 \times 10^{-2}\ s^{-1}$, Table 3) and a slightly different TOF value at 150 °C ($2.0 \times 10^{-2}\ s^{-1}$ and $2.4 \times 10^{-2}\ s^{-1}$, respectively). It is worth noting that the TOF values presented above are very similar to the TOF values previously reported ($2.04 \times 10^{-2}\ s^{-1}$, for $Ru3/Al_2O_3$ and $2.70 \times 10^{-2}\ s^{-1}$, for $Ru7/Al_2O_3$, both measured at 100 °C and 5 bar [13]) for catalysts prepared via the same colloidal method and with the same Ru loading of catalyst used in the present work. This confirms the reproducibility of catalysts and the role of size of particle distribution in catalytic performances. TEM analyses of $Ru3/Al_2O_3$ and $Ru7/Al_2O_3$ catalysts showed that they contain a more or less narrow size distribution (standard deviation of 0.9 nm). The heterogeneity in nanoparticle size is clearly demonstrated. Ru nanoparticles in the range 3–6 nm, were detected on $Ru3/Al_2O_3$, while particles in the range 2–5 nm were found on $Ru7/Al_2O_3$ catalyst. Therefore, $Ru3/Al_2O_3$ and $Ru7/Al_2O_3$ catalysts contain Ru particles with a similar size distribution, in spite of the different mean sizes. This seems to explain the similar TOF values obtained for both samples, considering that the catalytic activity was found to highly depend on the size distribution of Ru nanoparticles [12,13–15].

Concerning the oxidation state of Ru nanoparticles, all single catalysts present about the same surface percentage of metallic Ru after reduction and catalytic test (ST) (Fig. 12). Then, the higher activity of $Ru5/Al_2O_3$ catalyst cannot be explained by a higher percentage of metallic Ru. Actually, the differences in TOF values can be mostly assigned to the differences in the mean size and size distribution of Ru nanoparticles. A high catalytic activity is reached for Ru nanoparticles with a broad distribution of sizes and a relatively high mean size.

It has been argued [23] that hydrogen chemisorption over supported ruthenium crystallites became activated in the presence of chlorine adatoms apparently due to an electronic perturbation of the metal by chlorine. A crystallite size effect has been observed during the activated adsorption of hydrogen on supported ruthenium catalysts. This effect does not occur in the absence of adsorbed chlorine and is increasingly more pronounced as metal dispersion is increased. Preferential adsorption of chlorine atoms at high coordination sites reduces electron density at adjacent low coordination sites, thereby increasing the activation energy barrier for electron donation to, and dissociative chemisorption of, incoming hydrogen molecules. In the present work we used colloidal method for the deposition of Ru on the alumina. It has been demonstrated [18] that the colloidal synthesis of RuO2 nanoparticles followed by deposition on alumina is highly effective in Cl elimination. We didn't find traces of Cl by XPS analysis of the catalysts. Then the influence of traces of residual chlorine in our results seems to be completely excluded.

4.1.2. Effect of ammonia treatment (in absence or presence of hydrogen) on ammonia synthesis

4.1.2.1. Ammonia treatment in absence of hydrogen (NH_3 test) – ammonia. The proof of the decomposition of ammonia under the soft reactions conditions used in this work, is given by the presence of the two peaks corresponding to the products of the decomposition, namely hydrogen and nitrogen. In spite that the study was only qualitative (intensities of peaks are under the limit of quantification), for the three catalysts studied ($Ru3/Al_2O_3$, $Ru5/Al_2O_3$ and$Ru7/Al_2O_3$), the peak attributed to hydrogen was observed at 50 °C, 100 °C and 150 °C in the chromatogram after 2 min. The peak attributed to nitrogen is also observed at 2.4 min. Both peaks are more important at 150 °C.

4.1.2.2. The effect of ammonia treatment in absence of hydrogen on ammonia synthesis (NH_3 test + ST). The inhibitory effect of ammonia in the catalytic activity of ammonia synthesis was confirmed for all single catalysts (Fig. 9). N_2 conversion decreased between 20% and 35% after treating the catalysts under NH_3 flow. The inhibitory effect is more significant for the catalyst with highest activity in ammonia synthesis ($Ru5/Al_2O_3$), having a mean size of Ru nanoparticles of 6.9 nm. The NH_3 pretreatment of reduced catalysts also inhibits the reduction of RuO_2 under ammonia synthesis conditions (ST) (Fig. 12).

The B_5-type sites have been found to be the most energetically favorable sites for N_2 dissociation, commonly accepted as the rate-determining step of ammonia synthesis. In Fig. 7 is experimentally demonstrated that in sample $Ru7/Al_2O_3$ there is formation of the B_5-type sites after reduction and standard test (ST). The B_5-type sites are step sites exposing a three-fold hollow site close together with a bridge site [24–26]. The maximum concentration of B_5-type sites can be found in Ru particles of around 2–3 nm [27]. At low temperatures, NH_x intermediates of ammonia synthesis reaction

are strongly adsorbed on stepped surfaces (Fig. 7), which include B_5-type sites as well as their surrounding steps sites. Concerning hydrogen activation, the lowest adsorption energy allowing hydrogen dissociative adsorption has been found for the three-fold hollow sites on Ru(001) terraces, which are mostly exposed by large Ru nanoparticles [24].

Results suggests that during NH_3 treatment, NH_3 is adsorbed and dissociated on Ru particles ($NH_3 + * = NH_3*$, $NH_3* + * = NH_2* + H*$, etc.), which leads to the same NH_x intermediates than in ammonia synthesis [28]. Part of the NH_x intermediates could remain strongly adsorbed on the stepped surfaces exposed by small Ru particles, being hard to hydrogenate during low-temperature ammonia synthesis conditions. These NH_x species would directly block active sites for ammonia synthesis, or affect their local environment, leading to the decrease in the catalytic activity. These adsorbed NH_x species would additionally inhibit the reduction of RuO_2 to metallic Ru, by affecting the interaction of hydrogen with Ru particles or the mobility of hydrogen atoms along the surface. The higher NH_3 inhibitory effect observed for $Ru5/Al_2O_3$, which is the most active catalyst, suggests that the Ru particles present in this catalyst allow a stronger adsorption of NH_x intermediates formed during ammonia decomposition. The effect of Ru particle size on NH_x adsorption will be discussed later.

It can be assumed that during a conventional catalytic test of ammonia synthesis (without NH_3 pretreatment), part of the ammonia produced is decomposed on Ru particles, leading to NH_x intermediates strongly bound to stepped surfaces, which cannot be easily hydrogenated. The resulting deactivation of Ru sites for ammonia synthesis is more significant at higher temperatures and for catalysts with high concentration of stepped metal surfaces, that is, low concentration of large Ru nanoparticles. In consequence, it is favorable to carry out ammonia synthesis reaction under low temperatures and with catalysts having moderate Ru contents.

4.1.2.3. Ammonia treatment in presence of hydrogen ($NH_3 + H_2$ test) – inhibition of ammonia decomposition. For all single catalysts, no ammonia decomposition was detected during NH_3 treatment in presence of hydrogen, at 100 °C and 150 °C (no N_2 peak was observed). That is, hydrogen inhibits the decomposition of NH_3, at low temperatures. The presence of hydrogen might avoid a strong adsorption of NH_x intermediates on Ru nanoparticles, facilitating their hydrogenation. Hydrogen atoms adsorbed near the active sites for NH_x adsorption can actually modify their local environment, inducing lower adsorption energy of NH_x, and thus, an easier hydrogenation of these species.

4.1.2.4. The effect of ammonia treatment in presence of hydrogen on ammonia synthesis (NH_3+H_2 test + ST). The pretreatment of catalysts under NH_3 flow has an inhibitory effect on the catalytic activity of ammonia synthesis, even when the pretreatment is performed in presence of hydrogen, which has shown to inhibit NH_3 decomposition. At 100 °C, the activity decreases in about 10%, compared to the activity achieved without NH_3 pretreatment, but at 150 °C, it remains almost unchanged. This effect seems to be independent on the size of Ru nanoparticles, which is consistent with the fact that all single catalysts mostly contain small Ru particles exposing stepped surfaces, favoring the strong adsorption of NH_x intermediates. The presence of hydrogen weakens the adsorption of NH_x intermediates, which can be more easily hydrogenated.

The percentage of metallic Ru after the catalytic test significantly increases when the catalysts are previously exposed to NH_3 treatment in presence of hydrogen (Fig. 12). However, this increase of metallic Ru fraction does not result in a similar increase of the catalytic activity. Actually, at 150 °C, the activity obtained after NH_3 pretreatment in presence of hydrogen is almost the same than the one obtained without NH_3 pretreatment (Fig. 10). A high concentration of metallic Ru does not guarantee a high catalytic activity. It has been demonstrated that the activity mostly depends on the size distribution of Ru nanoparticles, the proximity between small and larger nanoparticles and the cooperative effects between them.

In conclusion, the presence of hydrogen has shown to inhibit ammonia decomposition during NH_3 treatment of catalysts at 100 °C and 150 °C, by inducing lower adsorption energy of NH_x intermediates and hydrogenating these species. Remaining NH_x intermediates can be easily hydrogenated during the subsequent ammonia synthesis reaction, which prevents the deactivation of Ru sites for ammonia synthesis.

Two important observations arise from the results: (1) the size distribution of Ru particles might affect the inhibitor role of hydrogen in ammonia decomposition. It has been previously demonstrated that the size of Ru nanoparticles has an important effect on the dissociative adsorption of hydrogen, and its capacity to move along the surface and hydrogenate.

Large Ru nanoparticles have shown to more easily activate hydrogen atoms with high mobility, which can migrate towards nearby small Ru nanoparticles. Therefore, large Ru nanoparticles might play an important role in providing hydrogen atoms allowing to prevent a strong adsorption of NH_x intermediates and to inhibit ammonia decomposition; (2) in absence of mobile H atoms, the strongly adsorbed NH_x intermediates can lead to the deactivation of the Ru sites involved in ammonia synthesis. As mentioned above, the presence of large particles is necessary to reach and keep a high catalytic of ammonia synthesis.

4.2. Mechanical mixtures of single catalysts ($Mix3 + 5/Al_2O_3$ and $Mix3 + 7/Al_2O_3$)

The reduction of RuO_2 after exposing the mixtures to reduction pretreatment and standard catalytic test was confirmed by XRD and XPS analyses, as in the case of single catalysts. The Ru particle sizes measured by XRD analysis of mixtures (16.5 nm for $Mix3 + 5/Al_2O_3$ and 17.3 nm for $Mix3 + 7/Al_2O_3$) are similar to the expected values corresponding to the average of the Ru sizes separately measured for both catalysts constituting the mixture (18.5 nm for $Mix3 + 5/Al_2O_3$ and 17.4 nm for $Mix3 + 7/Al_2O_3$). After reduction and standard test, a decrease in the size of Ru particles was detected by XRD, while XPS showed a slight decrease in the surface concentration of Ru atoms relative to Al atoms, indicating that the number of Ru atoms exposed at the surface do not significantly increase.

The XPS $(Ru/Al)_{exp}$ atomic ratio for the fresh mixtures is about the average of the values of the parent catalysts suggesting that the fresh mixtures of separated catalysts ($Ru3/Al_2O_3 + Ru5/Al_2O_3$ and $Ru3/Al2O3 + Ru7/Al_2O_3$) have been made without any modification of the separately prepared catalysts. Then no chemical contamination or formation of a new crystalline phase or increase in the covering of the surface of the support by Ru can be evoked to explain the catalytic activity of the mixture. The mixtures of the two catalysts are formed by the particles of the two catalysts, well mixed and in intimate contact. However after reduction and standard test the XPS $(Ru/Al)_{exp}$ atomic ratio are lower compared to the values of the parent catalysts. Clearly, there is an impoverishment in Ru on the surface. This result is confirmed by XRD. As a first explanation, differences could be due to the different surface configuration of the Ru nanoparticles in the mixture. From Fig. 5 it is observed that the efficacy in the reduction treatment (metallic Ru° formation) is in the order $Ru3/Al_2O_3 > Ru5/Al_2O_3 > Ru3/Al_2O_3$ (namely the increase in the reduced Ru corresponds to 180%, 140% and 68%, respectively, of the initial reduced Ru species). Namely large Ru particles are less prone to reduce during the reduction process, suggesting that the new configuration in the mixed catalysts corresponds to catalyst with larger Ru particles preferentially covering catalyst with

smaller Ru particles. As the XPS $(Ru/Al)_{exp}$ atomic ratio for the fresh mixtures is about the average of the values of the parent catalysts, the decrease in the XPS $(Ru/Al)_{exp}$ atomic ratio after reduction and ST, suggests that the overlap of the catalyst containing smaller Ru particles by the catalysts containing larger ones is realized during these two processes. This overlap leads to a decrease of the number of sites able to get reduced, which are situated mostly in smaller Ru nanoparticles, and thus to a decrease of the efficacy of the reduction process. Hydrogen activated in large Ru nanoparticles is not able to reduce all the sites on smaller Ru nanoparticles. This observation supports the fact that hydrogen migration of H atoms from large to small Ru nanoparticles is an important process in catalytic activity.

4.2.1. Synergy in the catalytic activity of mixtures – standard test

Mixtures present higher activity in ammonia synthesis than the single catalysts forming part of them. A synergistic effect in the catalytic activity results from the mixture of two catalysts having different mean sizes of Ru nanoparticles (Table 3). This effect depends on the temperatures and the sizes of Ru particles in the catalysts mixed. The explanation of the synergistic effect resides in the broader size distribution of Ru particles contained in the mixtures, compared to single catalysts, which has been confirmed previously [13]. Ammonia synthesis is better conducted on alumina surfaces having a broad size distribution of Ru nanoparticles, where small and larger particles in close proximity, give rise to a catalytic cooperation process [12,13–15].

DRIFTS analysis and H/D isotopic exchange studies showed that hydrogen is slowly activated and strongly attached to small Ru nanoparticles, leading to a reaction rate limited by the hydrogenation of NH_x intermediates. Larger Ru nanoparticles allow the activation of mobile hydrogen atoms that can more effectively hydrogenate NH_x intermediates [13,15]. It has been proposed that the catalytic cooperation mechanism between different-sized particles involves the migration of H atoms from large to small Ru nanoparticles (via surface hydroxyls), promoting the hydrogenation of the strongly adsorbed NH_x intermediates, which are directly blocking the active sites for ammonia synthesis or affecting their local environment. This is in agreement with the results presented in this work.

The percentage of metallic Ru increases with the reduction treatment and subsequent catalytic test (ST), reaching slightly lower percentages (30–40%) than those detected in single catalysts (40–50%). The different surface configuration of mixtures might result in a less effective reduction processes. In spite of the lower percentage of metallic Ru, the mixtures are more active in ammonia synthesis than single catalysts. As mentioned before, the catalytic activity mostly depends on the surface configuration of Ru catalysts, that is, the mean size and size distribution of Ru particles, and the proximity between particles of different sizes.

4.2.2. The inhibitor role of ammonia

As in the case of single catalysts, ammonia treatment drastically inhibits the catalytic activity of mixtures in ammonia synthesis (Table 5). After ammonia pretreatment in absence of hydrogen, the drop in the activity of mixtures (about 50–60%) is higher than for single catalysts (15–30%), while the surface percentage of metallic Ru is similar in mixtures and single catalysts (in the order of 20–40%). As proposed for single catalysts, NH_x intermediates are strongly bound to stepped surfaces, including the most active sites for N_2 adsorption (B_5 sites) and their neighboring sites. When NH_3 is stopped and the catalyst is exposed to ammonia synthesis conditions, the strongly adsorbed NH_x intermediates inhibit the reaction by directly blocking the active sites or affecting their local environment. The drop in the catalytic activity after ammonia treatment (in absence of hydrogen) is higher for the mixtures than for single catalysts. This can be explained by an additional inhibitory effect of ammonia adsorption on the acid alumina surface sites, strongly affecting the mechanism of catalytic cooperation (e.g. hydrogen transfer) between different-sized Ru nanoparticles, which has shown to keep the high catalytic performance of mixtures during low-temperature ammonia synthesis.

After NH_3 treatment in presence of hydrogen, the catalytic performance of mixtures also decreases, but in a much lower extent (about 15%) than in absence of hydrogen 5 (Table 6). This confirms the inhibitor effect of hydrogen on ammonia decomposition, thus preventing the catalyst deactivation by adsorbed NH_x intermediates. The transfer of hydrogen that is known to occur at the surface of mixtures certainly contributes to a more effective hydrogenation of the strongly adsorbed NH_x intermediates.

The activity of mixtures in ammonia synthesis is not fully recovered after $NH_3 + He + H_2$ treatment, leading to reaction rates still lower than those obtained without ammonia treatment. This means that, even in presence of hydrogen, the exposure to ammonia leads to certain deactivation of the mixtures. It is possible that some NH_x intermediates adsorbed on low-coordination Ru sites exposed on very small Ru particles cannot be hydrogenated, despite the transfer of hydrogen atoms continuously taking place on the surface of mechanical mixtures. Probably, a closer proximity between small and large Ru nanoparticles and a higher concentration of large Ru nanoparticles would lead to a more effective hydrogenation of NH_x intermediates and, eventually, to a full recovery of the catalytic performance of mixtures.

It could be argued that ammonia can titrate the support, which may be also the reason of the dramatic loss of the activity afterwards. The results presented in this work seem to give arguments to support this explanation. As indicated above [15], diffusion of hydrogen on $Ru/\gamma\text{-}Al_2O_3$ catalysts was studied by H/D isotopic exchanges starting from D_2 in the gas phase (heteroexchange). H/D exchange was shown to occur under temperature conditions (83 °C) where direct exchange between gas phase and alumina was completely discarded. This proves that D atoms activated on both small and larger Ru particles, are actually transferred to alumina support and exchanged with hydrogen atoms from OH groups. In situ DRIFTS analysis provides irrefutable evidence of this exchange: characteristic stretching vibrations of OH and OD groups appear with an isotope ratio of $\nu OH/\nu OD$ 1.356. A much faster H/D isotopic exchange was reached over large Ru supported nanoparticles, meaning that those particles do not only promote dissociative adsorption of hydrogen, but also lead to a higher diffusivity of hydrogen atoms on the catalytic surface. The lower hydrogen diffusivity on small Ru nanoparticles is in agreement with the highly strong H-metal bonds formed during hydrogen adsorption, which inhibits the mobility of hydrogen atoms [15]. The fact that ammonia titrate the hydroxyl groups decreases the efficacy of the transfer of hydrogen from larger to smaller particles, then decreasing (dramatically) the catalytic performances. This underlines again the importance of the cooperation between Ru particles of different size and the hydrogen migration in the catalyst in the catalytic activity.

The interaction between adsorbed atoms (hydrogen and possible impurities (such as sulfur and chloride)) can strongly affect the strength of hydrogen adsorption. In particular, attractive or repulsive lateral forces can be exerted between adjacent adsorbed hydrogen atoms, depending on their surface concentration (hydrogen coverage). When the adsorption of a hydrogen atom involves more than one metal site, adsorbing a second hydrogen atom in the vicinity implies sharing the electronic charge of all metal atoms involved. This affects the strength of the hydrogen-metal bond and, eventually, the arrangement of chemisorbed hydrogen atoms on the surface. At high hydrogen coverage, the adsorption strength becomes weaker and the adjacent H atoms exhibit repulsive interactions [29–33]. Large Ru nanoparticles have shown to promote

hydrogen activation, probably by exposing a high concentration of the energetically favorable sites (three-fold hollow sites) for hydrogen dissociative adsorption. H poisoning of the reaction can be observed in small Ru particles. H atoms are strongly adsorbed to the low-coordination Ru sites exposed on small Ru nanoparticles. The surface structure with stepped terraces developed by large Ru nanoparticles is expected to expose high concentration of three-fold hollow sites, thus leading to a high hydrogen adsorption rate. The formation of large terraces while increasing the size of supported Ru nanoparticles has also been observed by AFM analysis [16]. Small nanoparticles meanwhile present a highly defective surface (with kinks and edges), mostly exposing low coordinated Ru sites that are expected to strongly bind hydrogen atoms (Fig. 7). A strong adsorption of H atoms on small Ru particles inhibits hydrogen mobility and its molecular desorption [15], which would lead to the low initial rate of hydrogen adsorption on these particles. The ability of activated H atoms to migrate from Ru metal particles towards the support was confirmed via H/D isotopic exchange experiments [15]. As discussed above, H atoms activated on Ru nanoparticles can be transferred to alumina and move along the surface via exchange with the hydrogen atoms from hydroxyl groups. The rate of H/D exchange is higher on surfaces containing large Ru nanoparticles and a synergy in hydrogen diffusivity occurs when mixing catalysts containing Ru nanoparticles with different sizes. For surfaces containing small and larger Ru nanoparticles, experimental evidence confirms that large Ru nanoparticles would participate as a source of mobile H atoms able to migrate towards small nanoparticles and to promote the diffusivity of hydrogen on their surface. As suggested above, these H atoms might be also able to hydrogenate NHx intermediates or modulate the strength of adsorption sites on small metal particles, thus promoting ammonia synthesis reaction.

5. Conclusions

The important effect of the average size and size distribution of Ru nanoparticles on the catalytic activity of ammonia synthesis has been confirmed. The most active catalysts present a broad size distribution of Ru nanoparticles. A high percentage of metallic Ru is necessary, but not sufficient, for a high activity.

Ammonia pretreatment of catalysts inhibits their performance during ammonia synthesis, and it also inhibits the reduction of oxidized ruthenium atoms on the surface. During NH_3 treatment, the decomposition of ammonia leads to NH_x intermediates strongly adsorbed on Ru stepped surfaces, including the most active sites for ammonia synthesis and the surrounding step sites. Under ammonia synthesis conditions, these NH_x intermediates remain adsorbed and inhibit the catalytic activity, by blocking active sites or affecting their local environment. When NH_3 treatment is performed in presence of hydrogen, ammonia decomposition is inhibited. Hydrogen induces lower adsorption energy of NH_x on small Ru particles, and thus, an easier hydrogenation of these intermediates. Therefore, NH_x intermediates are more easily hydrogenated during ammonia synthesis reaction, and the catalytic activity is not significantly affected. The inhibition of catalytic performances is more significant at higher temperatures and for catalysts with low concentration of large Ru nanoparticles, confirming that is favorable to carry out ammonia synthesis under low temperatures and with catalysts having an adequate size distribution of Ru particles.

The presence of large Ru nanoparticles is necessary to reach and keep a high activity during ammonia synthesis. Large Ru nanoparticles more effectively activate H atoms that are able to migrate towards small Ru nanoparticles, promoting the hydrogenation of NH_x intermediates. Mixing two catalysts with different mean sizes of Ru nanoparticles leads to an important synergistic effect in the catalytic activity.

Results reveal the importance of synthesizing catalysts with an adequate surface configuration (broad size distribution of Ru nanoparticles, high interdispersion of different-sized Ru particles and close proximity between particles) for the effective activation and transfer of hydrogen atoms, which is crucial to ensure the hydrogenation of NH_x intermediates and thus, a high activity during ammonia synthesis.

Acknowledgements

Authors gratefully acknowledge the financial support of the Belgium National Fund for Scientific Research (FSR-FNRS) and BECAS CHILE – CONICYT Ph.D. (CF) Fellowship Program of Chilean Government. TEM analyses were conducted at LCMCP – Laboratoire de Chimie de la Matière Condensée de Paris, Collège de France, Paris, France (Dr. C. Sassoye, Prof. C. Sanchez).

References

[1] O. Hinrichsen, F. Rosowski, A. Hornung, M. Muhler, G. Ertl, J. Catal. 165 (1997) 33–44.
[2] P. Seetharamulu, V. Siva Kumar, A.H. Padmasri, B. David Raju, K.S. Rama Rao, J. Mol. Catal. A 263 (2007) 253–258.
[3] A. Miyazaki, I. Balint, K.-i. Aika, Y. Nakano, J. Catal. 204 (2001) 364–371.
[4] K. Aika, A. Ohya, A. Ozaki, Y. Inoue, I. Yasumori, J. Catal. 92 (1985) 305–311.
[5] S. Wu, J. Chen, X. Zheng, H. Zeng, C. Zheng, N. Guan, Chem. Commun. 19 (2003) 2488–2489.
[6] C.J.H. Jacobsen, S. Dahl, P.L. Hansen, E. Törnqvist, L. Jensen, H. Topsøe, D.V. Prip, P.B. Møenshaug, I. Chorkendorff, J. Mol. Catal. A 163 (2000) 19–26.
[7] B. Lin, K. Wei, J. Lin, J. Ni, Catal. Commun. 39 (2013) 14–19.
[8] A.M. Karim, V. Prasad, G. Mpourmpakis, W.W. Lonergan, A.I. Frenkel, J.G. Chen, D.G. Vlachos, J. Am. Chem. Soc. 131 (2009) 12230–12239.
[9] Z. Kowalczyk, S. Jodzis, W. Raróg, J. Zieliński, J. Pielaszek, A. Presz, Appl. Catal. A 184 (1999) 95–102.
[10] W. Raróg-Pilecka, E. Miśkiewicz, D. Szmigiel, Z. Kowalczyk, J. Catal. 231 (2005) 11–19.
[11] C. Liang, Z. Wei, Q. Xin, C. Li, Appl. Catal. A 208 (2001) 193–201.
[12] C. Fernández, C. Sassoye, D.P. Debecker, C. Sanchez, P. Ruiz, Appl. Catal. A 474 (2014) 194–202.
[13] C. Fernández, C. Pezzotta, E.M. Gaigneaux, N. Bion, D. Duprez, P. Ruiz, Catal. Today 251 (2015) 88–95.
[14] C. Fernández, C. Sassoye, N. Flores, N. Escalona, C. Sanchez, P. Ruiz, Appl. Catal. A 502 (2015) 48–56.
[15] C. Fernandez, N. Bion, E. Gaigneaux, D. Duprez, P. Ruiz, J. Catal. 344 (2016) 16–28.
[16] C. Fernández, C. Pezzotta, G. Raj, E.M. Gaigneaux, P. Ruiz, Catal. Today 259 (2016) 183–191.
[17] C. Sassoye, G. Muller, D.P. Debecker, A. Karelovic, S. Cassaignon, C. Pizarro, P. Ruiz, C. Sanchez, Green Chem. 13 (2011) 3230–3237.
[18] R. Wojcieszak, M.J. Genet, P. Eloy, P. Ruiz, E.M. Gaigneaux, J. Phys. Chem. C 114 (2010) 16677–16684, 16677.
[19] F.P.J.M. Kerkhof, J.A. Moulijn, J. Phys. Chem. 83 (1979) 1612–1619.
[20] J.H. Scofield, J. Electron. Spectrosc. Relat. Phenom. 8 (1976) 129–137.
[21] S. Tanuma, C.J. Powell, D.R. Penn, Surf. Interface Anal. 21 (1994) 165–176.
[22] S. Tougaard, QUASES-IMFP-TPP2 M, QUASES-Tougaard Inc, Denmark, 2002.
[23] W.I.K. Lu, B.J. Tatarchuk, J. Catal. 106 (1987) 176–187.
[24] S. Dahl, E. Törnqvist, I. Chorkendorff, J. Catal. 192 (2000) 381–390.
[25] J.K. Honkala, A. Hellman, I. Remediakis, A. Logadottir, A. Carlsson, S. Dahl, C.H. Christensen, J.K. Nørskov, Science 307 (2005) 555–558.
[26] S. Dahl, A. Logadottir, R.C. Egeberg, J.H. Larsen, I. Chorkendorff, E. Törnqvist, J.K. Nørskov, Phys. Rev. Lett. 83 (1999) 1814–1817.
[27] C.J.H. Jacobsen, S. Dahl, P.L. Hansen, E. Törnqvist, L. Jensen, H. Topsøe, D.V. Prip, P.B. Møenshaug, I. Chorkendorff, J. Mol. Catal. A 163 (2000) 19–26.
[28] A. Hellmann, J.K. Honkala, I. Remediakis, A. Logadottir, A. Carlsson, S. Dahl, C.H. Christensen, J.K. Nørskov, Surf. Sci. 600 (2006) 4264–4268.
[29] K. Christmann, Surf. Sci. Rep. 9 (1988) 1–163.
[30] K.H. Rieder, W. Stocker, Surf. Sci. 164 (1985) 55–84.
[31] J.M. Campbell, C.T. Campbell, Surf. Sci. 259 (1991) 1–17.
[32] M. Kiskinova, D.W. Goodman, Surf. Sci. 108 (1981) 64–76.
[33] J.L. Brand, A.A. Deckert, S.M. George, Surf. Sci. 194 (1988) 457–474.